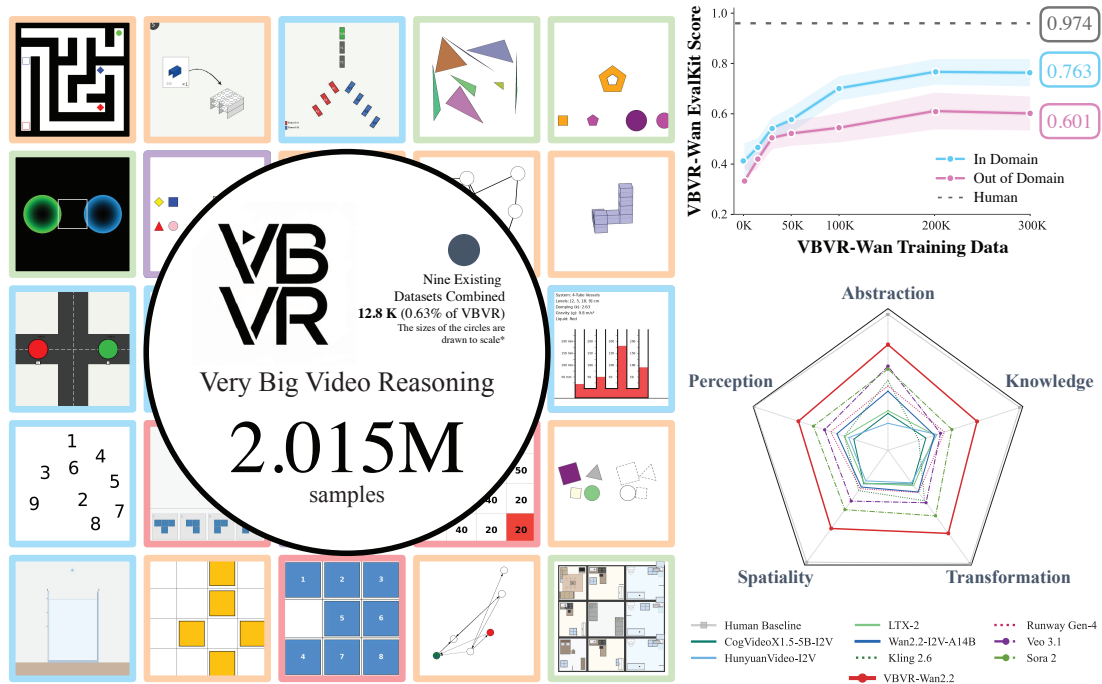


A Very Big Video Reasoning Suite

Maijunxian Wang*¹ Ruisi Wang*² Juyi Lin*³ Ran Ji*⁴ Thaddäus Wiedemer⁵ Qingying Gao⁶
 Dezhi Luo⁷ Yaoyao Qian³ Lianyu Huang⁸ Zelong Hong⁹ Jiahui Ge⁸ Qianli Ma¹⁰ Hang He¹¹
 Yifan Zhou¹⁰ Lingzi Guo¹² Lantao Mei¹² Jiachen Li¹³ Hanwen Xing⁸ Tianqi Zhao¹⁴
 Fengyuan Yu² Weihang Xiao¹⁵ Yizheng Jiao¹⁶ Jianheng Hou⁸ Danyang Zhang¹⁷
 Pengcheng Xu¹⁸ Boyang Zhong¹⁹ Zehong Zhao⁴ Gaoyun Fang²⁰ John Kitaoka²¹ Yile Xu²²
 Hua Xu²³ Kenton Blacutt²⁴ Tin Nguyen²⁵ Siyuan Song¹³ Haoran Sun⁶ Shaoyue Wen²⁰
 Linyang He²⁶ Runming Wang⁶ Yanzhi Wang³ Mengyue Yang²⁷ Ziqiao Ma⁷ Raphaël Millière²⁸
 Freda Shi²⁹ Nuno Vasconcelos⁴ Daniel Khashabi⁶ Alan Yuille⁶ Yilun Du³⁰ Ziming Liu¹²
 Bo Li² Dahua Lin³¹ Ziwei Liu² Vikash Kumar³² Yijiang Li⁴ Lei Yang³¹
 Zhongang Cai^{2†} Hokin Deng^{32†}

¹ University of California, Berkeley ² Nanyang Technological University ³ Northeastern University ⁴ University of California, San Diego ⁵ University of Tübingen ⁶ Johns Hopkins University ⁷ University of Michigan ⁸ University of Southern California ⁹ Washington University in St. Louis ¹⁰ Shanghai Jiao Tong University ¹¹ East China Normal University ¹² Stanford University ¹³ University of Texas at Austin ¹⁴ University of California, Los Angeles ¹⁵ Cornell University ¹⁶ University of North Carolina at Chapel Hill ¹⁷ San Jose State University ¹⁸ University of California, Irvine ¹⁹ Technical University of Munich ²⁰ Imperial College London ²¹ University of Wisconsin–Madison ²² University of Edinburgh ²³ Hong Kong University of Science and Technology ²⁴ New York University ²⁵ Auburn University ²⁶ Columbia University ²⁷ University of Bristol ²⁸ University of Oxford ²⁹ University of Waterloo ³⁰ Harvard ³¹ The Chinese University of Hong Kong ³² Carnegie Mellon University *Equal contribution. [†] Correspondence to: Hokin Deng <hokind@andrew.cmu.edu>, Zhongang Cai <caiz0023@e.ntu.edu.sg>.

Figure 1 Overview of VBVR. Left: the grid shows representative tasks spanning our cognitive architecture, which are color-coded according to their underlying capability: **Spatiality**, **Transformation**, **Knowledge**, **Abstraction**, and **Perception**. At the center of the grids, we visualize the scale comparison between VBVR (2.015M samples) and nine other datasets combined (12.8K samples): the sizes of the circles are drawn to scale. Top-right: scaling behavior on in-domain and out-of-domain evaluations. Bottom-right: benchmark performance across five cognitive capabilities.



ABSTRACT

Rapid progress in video models has largely focused on visual quality, leaving their reasoning capabilities underexplored. Video reasoning grounds intelligence in spatiotemporally consistent visual environments that go beyond what text can naturally capture, enabling intuitive reasoning over spatiotemporal structure, such as continuity, interaction, and causality. However, systematically studying video reasoning and its scaling behavior is hindered by the lack of large-scale video reasoning training data. To address this gap, we introduce the **Very Big Video Reasoning (VBVR) Dataset**, an unprecedentedly large-scale resource spanning 200 curated reasoning tasks following a principled taxonomy, and over *one million* video clips—approximately *three orders of magnitude* larger than existing datasets. We further present **VBVR-Bench**, a verifiable evaluation framework that moves beyond model-based judging by incorporating rule-based, human-aligned scorers, enabling reproducible and interpretable diagnosis of video reasoning capabilities. Leveraging the VBVR suite, we conduct one of the first large-scale **scaling studies** of video reasoning and observe early signs of emergent generalization to unseen reasoning tasks. Together, VBVR lays a foundation for the next stage of research in generalizable video reasoning. The data, benchmark tool kit, and models are released publicly at video-reason.com.

1. Introduction

Ground-breaking progress has been achieved in large language models, whose reasoning abilities now generalize across challenging tasks such as coding, mathematics, and scientific discovery (Mitchell, 2025; Rapaport, 2026). However, such capabilities remain largely confined to text-based scenarios. Meanwhile, recent advances in video generation models have predominantly emphasized visual realism, with comparatively limited focus on reasoning capabilities. Yet video models hold the potential to support a new paradigm of reasoning (Wiedemer et al., 2025), grounded in spatiotemporally consistent visual environments where spatial structure, physical dynamics, and long-range causality are naturally encoded. This makes video frames an ideal substrate for studying reasoning grounded in the physical world. Despite this promise and growing interest in video reasoning, the community still lacks several critical components required for systematic progress: (1) a large-scale and diverse **dataset** to enable meaningful investigation of scaling and generalization, (2) an **evaluation toolkit** built on verifiable and reproducible principles, and (3) an initial **scaling study** that examines emergent capabilities in video reasoning models. In this work, we address all three challenges by introducing the **Very Big Video Reasoning (VBVR)** suite.

First, we introduce **VBVR-Dataset**, a large-scale and diverse training source designed to facilitate systematic study of video reasoning. We adopt a principled approach, grounding our task taxonomy in well-established theories of human cognitive architecture (Newell & Simon, 1972; Anderson, 2007). Specifically, we organize core visual reasoning capabilities into five pillars: *abstraction*, *knowledge*, *spatiality*, *perception*, and *transformation*. The dataset is the result of a community-oriented, collaborative effort involving over 50 researchers and engineers from diverse disciplines worldwide, ensuring broad coverage and strong domain expertise across 200 tasks to date. Contributors are given full freedom to design the core task semantics and reasoning procedures, allowing for maximal diversity, while a unified, overarching task template is applied as a standardized wrapper for input and output specification. This separation ensures consistency for automated scaling without constraining task creativity. All tasks undergo expert human inspection to ensure quality and correctness before being processed by our automated, cloud-based pipeline, which generates large volumes of randomized training examples in a distributed manner. In total, VBVR-Dataset contains 2,015,000 images and 1,007,500 video clips, making it approximately $1,000\times$ larger than existing alternatives. Importantly, the pipeline is immediately compatible with newly added tasks and supports scalable generation of additional examples per task, enabling continuous expansion in both dataset breadth and scale.

Second, **VBVR-Bench** provides a systematic, reproducible, and explainable evaluation framework for video reasoning models. While VLM-as-a-judge paradigms have been widely adopted for evaluating video generation models (Peng et al., 2025), we explicitly enforce the use of verifiable, rule-based scorers to ensure that

Table 1 Comparison of VBVR-Dataset with existing video reasoning benchmarks. VBVR-Dataset surpasses all prior benchmarks by multiple orders of magnitude across every dimension and is, to our knowledge, the first to provide large-scale training data for video reasoning.

Dataset	#Task	#Images	#Videos	#Train	#Test
Video-Zero-Shot (Wiedemer et al., 2025)	69	1,578	0	0	2,128
V-ReasonBench (Luo et al., 2025c)	13	652	0	0	326
MMGR (Cai et al., 2025)	10	1,323	530	0	1,853
VideoThinkBench (Tong et al., 2025)	24	8,298	0	0	4,149
TiViBench (Chen et al., 2025)	24	595	0	0	595
VR-Bench (Yang et al., 2025a)	5	0	7,920	6,336	1,538
MME-CoF (Guo et al., 2025)	12	120	0	0	120
Gen-ViRe (Liu et al., 2025)	24	117	0	0	72
Ruler-Bench (He et al., 2025)	40	101	0	0	622
VBVR-Dataset	200	2,015,000	1,007,500	1,000,000	7,500

Table 2 Foundational faculties of a human mind. One-sentence definitions are provided. The comprehensive set of philosophical justifications and empirical supports for each faculty are available in App. A.

Faculty	Definition
Abstraction	To find rules from observations and use rules to deduce results.
Knowledge	Propositional truth statements one could utter, either learned or gifted since birth.
Perception	Immediate access to sense datum, no further justification could be provided, i.e. "Here is one hand"
Spatiality	The intuition of the basic properties of our world, such as three-dimensionality and Euclidean-ness.
Transformation	To simulate spatial-temporal continuities with internal models in one's mind

evaluation outcomes are clearly defined and fully reproducible. To validate that these task-specific scorers faithfully reflect model capabilities, we conduct human preference alignment experiments, observing strong agreement between automated scores and human judgments, with a Spearman’s correlation coefficient of $\rho > 0.9$. Leveraging VBVR-Bench, we benchmark leading proprietary models: Veo 3.1 (Google DeepMind, 2026), Sora 2 (OpenAI, 2025), Kling 2.6 (Kuaishou Technology, 2025), and Runway Gen-4 (Runway Research, 2025), alongside representative open-source models, including Wan-2.2 (WanTeam, 2025), CogVideoX-1.5 (Yang et al., 2024), HuanyuanVideo (Kong et al., 2024), and LTX-2 (HaCohen et al., 2026). We reveal a substantial gap in video reasoning capabilities across systems; the strongest model still falls short of human performance by a large margin. Moreover, we use VBVR to analyze how different cognitive capabilities co-develop across models, revealing non-trivial dependencies and trade-offs between reasoning skills.

Third, with a large-scale dataset and a reliable evaluation benchmark in place, we conduct an in-depth investigation of scaling effects in video generation models. Using Wan-2.2 as the base model, we observe concurrent performance improvements on both in-domain (ID) and out-of-domain (OOD) tasks as training scale increases, indicating the gradual emergence of generalization capabilities. Beyond these gains, our analysis yields several key insights. First, performance on both ID and OOD tasks eventually plateaus as data scale increases, leaving a persistent gap between model and human performance that cannot be bridged by data scaling alone. This suggests fundamental limitations in current video generation architectures when applied to video reasoning. Second, although OOD performance improves substantially with scale, a consistent gap remains between ID and OOD settings; narrowing this gap appears essential for robust, in-the-wild video reasoning and generation. Finally, qualitative analyses reveal emergent behaviors in instruction following, controlled editing, and semantic understanding with increased model scale, while also exposing important limitations that motivate future research.

In summary, we present the VBVR suite, centered on an unprecedentedly large-scale and continually growing dataset for video reasoning, **VBVR-Dataset**, together with a verifiable, human-aligned evaluation toolkit, **VBVR-Bench**. Leveraging this suite, we conduct one of the first systematic scaling studies of video reasoning models and uncover early, encouraging evidence of emergent generalization. We believe VBVR provides a foundational infrastructure for future research toward generalizable video reasoning.

2. Related Works

Since the inauguration of diffusion models and transformer-based scaling (Ho et al., 2020; Peebles & Xie, 2023), video generation models are rapidly proliferating, with closed models such as Sora, MovieGen, and Veo, and open-source ones like CogVideoX, HunyuanVideo, and Wan (OpenAI, 2025; Polyak et al., 2024; Google DeepMind, 2026; Yang et al., 2024; Kong et al., 2024; WanTeam, 2025). But many models are optimized for creative production rather than explicit relational, causal, or counterfactual reasoning (Peebles & Xie, 2023; Yang et al., 2024; Zheng et al., 2024). A growing body of work treats video generation not only as a content-creation tool, but as a reasoning substrate (Tong et al., 2025; Guo et al., 2025; Liu et al., 2025; Wiedemer et al., 2025). A work has tested Veo-3 and shown early evidence that the model exhibits nontrivial zero-shot perceptual and manipulation behaviors and can solve simple tasks without task-specific training (Wiedemer et al., 2025). Later works now span generation-as-reasoning paradigms (Tong et al., 2025), multi-step Chain-of-Frame diagnosis (Guo et al., 2025; Liu et al., 2025), TI2V answer suites (Luo et al., 2025c; Chen et al., 2025), among others (He et al., 2025; Yang et al., 2025a; Cai et al., 2025).

Despite sharper measurement, much of the ecosystem remains evaluation-heavy: standardized, large-scale training splits and controlled ablation protocols are missing, making it difficult to run reproducible scaling studies that directly optimize for reasoning correctness. This motivates datasets that are designed not only to test video reasoning, but to support training for reasoning at scale under consistent domain coverage and reliable supervision signals.

3. Dataset

In this section, we describe the cognitive architecture underlying our systematic task design (Sec. 3.1), present the key statistics of VBVR-Dataset (Sec. 3.2), and detail the data generation pipeline (Sec. 3.3).

3.1. Cognitive Architecture

Aristotle treated cognition as an organized hierarchy of *dunamis*, cognitive faculties, ascending from *aisthēsis*, perception, through *phantasia*, imagination, and *mnēmōnē*, memory, to *noûs*, understanding, culminating in the extraction of *katholou*, knowledge, from *empeiria*, experience (Aristotle, 1984g;b). Kant further argued the mind structures experience through *a priori* intuitions and categories, aggregating by *Einbildungskraft* (Kant, 1781). Synthesizing from two millennia of philosophical inquiry and recent cognitive and neural sciences, we organize VBVR around five foundational cognitive faculties. **Perception** refers to the extraction of structured representations from sensory input, what Aristotle called receiving “form without matter”, where, for example, we test edge detection, color, and shape perception, discrimination (Aristotle, 1984g; Hubel & Wiesel, 1962; DiCarlo et al., 2012). **Transformation** is the manipulation and synthesis of mental representations, corresponding to Aristotle’s *phantasia* and Kant’s *Einbildungskraft*, where we use cases like mental rotation to test (Shepard & Metzler, 1971; Zacks, 2008). **Spatiality** is the representation of places and their geometric relationships in our world. Kant identified space as an *a priori* form of intuition prerequisite to perception itself, and we use cases like navigation to probe this ability (Kant, 1781; O’Keefe & Dostrovsky, 1971; Hafting et al., 2005). **Abstraction** is the distillation of generalizable knowledge from particular experiences, Aristotle’s *katholou* extracted by *noûs*, Kant’s transcendental ideas generated by *Vernunft*, and we use cases like Raven’s Matrices to test (Aristotle, 1984b; Kant, 1781; Carey, 2009; Badre & Nee, 2018). **Knowledge**, as Aristotle has referred, is the *telos* of human life. Through the faculties of our mind, humans accumulate and refine knowledge over time. This knowledge may be intrinsic, that is, foundational or core knowledge we are born with, or learned (Aristotle, 1984c;b;d;e; Spelke, 2000; Li et al., 2025). To operationalize these faculties in a video-based reasoning setting, VBVR implements each category as a family of parameterized task generators. Representative task instances for each faculty are illustrated in Fig. 2. Full philosophical grounding and neuroscientific evidence for each faculty appear in Sec. A.

Figure 2 Sample task instances generated from the VBVR parameterized task suite, organized by five cognitive faculties. Each sequence illustrates the structured reasoning process required to reach a valid solution. Tasks are implemented as deterministic generators supporting scalable instance variation while preserving visual clarity and video dependency. Each row corresponds to a faculty defined in Section 3.1: abstract cognitive constructs are instantiated as executable, verifiable video-based reasoning tasks.

Task 1 (Top Left): Multiple polygons are shown; exactly one of them is a pentagon (5 sides). Identify that pentagon and mark it with a red circle that expands from the inside out to encircle the shape. Do not change anything else.

Task 2 (Top Right): The scene contains two types of shapes, each type has three shapes of different sizes arranged randomly. Keep all shapes unchanged in appearance (type, size, and color). Only rearrange their positions: first group the shapes by type, then within each group, sort the shapes from smallest to largest (left to right), and arrange all shapes in a single horizontal line from left to right.

Task 3 (Middle Left): The scene shows four L-shaped pipes, each oriented at different angles. Rotate each L-shaped pipe as needed to connect all pipes and form a complete square frame. Only rotate the pipes that need adjustment; keep the others stationary. Show this process step by step until all pipes are properly connected into a square loop.

Task 4 (Middle Right): The scene shows two circles of the same color but different sizes at different positions. Keep both circles unchanged in size and color. Only move their positions. Move both circles until they share the same center point (concentric circles) exactly at the center of the image.

Task 5 (Bottom Left): The scene shows a 10x10 grid with a green start square (containing a red circular agent) and a purple end square. Starting from the green start square, the agent can move to adjacent cells (up, down, left, right) each step. The goal is to move the agent to the purple end square along the shortest path.

Task 6 (Bottom Middle): The scene shows a 15x15 grid maze with dark walls and white pathways. A green circular marker indicates the starting position, and a red flag marks the end position. Starting from the green start position, navigate through the maze by moving along the white pathways. You can move to adjacent cells (up, down, left, right) but cannot pass through the dark walls. The goal is to find and demonstrate the complete path from the green start to the red flag end position, showing each step of the journey through the maze.

Task 7 (Bottom Right): Complete this sliding puzzle. The goal is to arrange the numbered tiles in sequential order (filling each row from left to right, with rows from top to bottom), with the blank space at the bottom-right corner. Rules: Only tiles adjacent to the blank space can be moved. Slide one tile per move into the blank space. Complete in exactly 5 moves. Do not make extra moves. Keep the camera view fixed and maintain the grid structure unchanged.

Task 8 (Bottom Far Right): In the scene, there are 3 ball clusters: red cluster A has 4 balls, and there are other clusters with different numbers of balls. The global TOTAL label shows the sum 12. Control the red cluster A to absorb other clusters. You can only absorb clusters that are smaller than the red cluster. Find the correct sequence to absorb all clusters step by step until all balls become red.

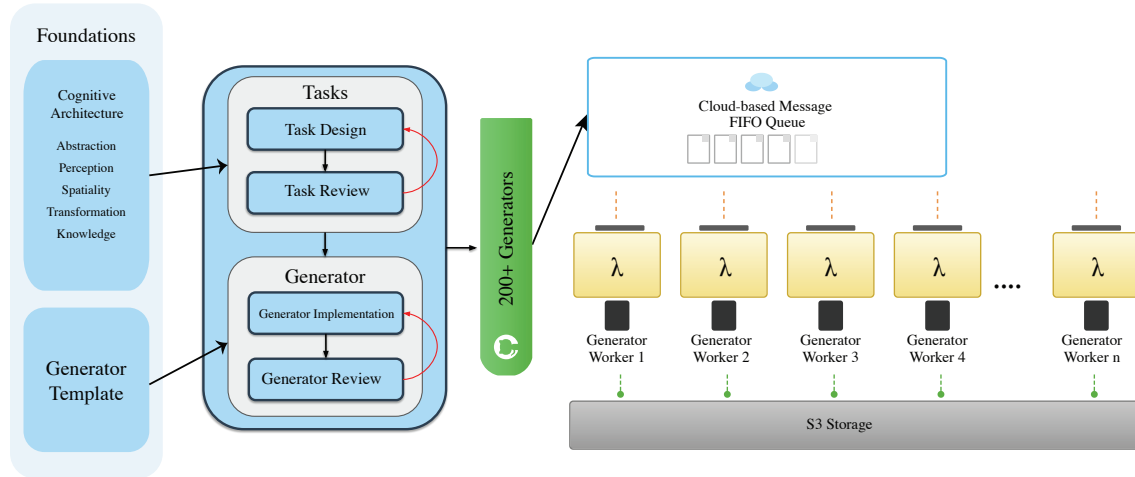
Task 9 (Bottom Far Left): The scene shows 5 numbered dots scattered across the image. Connect the dots in numerical order (1→2→3→4→5) by drawing red straight lines between them, one line at a time in sequence.

Task 10 (Bottom Far Right): A ball at height 19.6m with initial downward velocity 4.6 m/s falls under gravity 7.8 m/s² and bounces on ground with elasticity 0.80. Show the full trajectory with velocity arrows (direction and magnitude) updating throughout until the ball stops.

3.2. Data Statistics

Table 1 compares VBVR-Dataset with existing video reasoning benchmarks. VBVR-Dataset surpasses prior work by *multiple orders of magnitude* across all key dimensions. Notably, most existing video reasoning benchmarks provide few or no video samples (often lacking training data altogether), which has been a major bottleneck for studying scaling. In total, VBVR-Dataset comprises 200 tasks: 150 tasks will be publicly released, while the remaining 50 tasks are reserved as a hidden set for future leaderboard evaluation to preserve benchmark integrity.

Figure 3 Task designs grounded in cognitive architecture are implemented as parameterized generators, then executed at scale via distributed Lambda workers writing to centralized S3 storage.



3.3. Data Curation

The curation process follows a three-stage pipeline: (1) task design and approval, (2) task-specific generator implementation, and (3) large-scale distributed generation with quality control. Each stage produces well-defined outputs for downstream processing.

3.3.1. Task Design and Approval

Each task is designed to probe a specific video-based reasoning capability from the taxonomy defined in Sec. 3.1. Rather than relying on implicit or post-hoc task definitions, VBVR explicitly constrains the task space through a unified set of quality standards.

All task proposals are evaluated against six criteria: (1) **Information sufficiency**, requiring all necessary reasoning cues to be present in the first frame and the prompt; (2) **Deterministic solvability**, ensuring a unique and verifiable success criterion; (3) **Video dependency**, such that the task cannot be solved from a single static image but through a process; (4) **Visual clarity**, ensuring all visual elements are distinguishable with unambiguous layouts; (5) **Parametric diversity**, supporting the generation of at least 10,000 non-trivial instances; (6) **Technical feasibility**, avoiding unsolvable or pathological configurations under standard rendering pipelines.

Task proposals are submitted by internal contributors and the open-source community. Each proposal specifies the reasoning objective, expected input–output structure, and parameter space. Proposals undergo a design review process conducted by designated reviewers, who assess cognitive validity, verifiability, and scalability. Through this rigorous review process, slightly more than **200 task designs** have already been approved from over 500 initial proposals. Only approved tasks proceed to implementation.

3.3.2. Task-Specific Generator Implementation

The second stage implements approved designs as executable generators. Each approved task design is implemented as a task-specific parameterized generator. For example, a grid navigation generator produces diverse task instances by specifying different grid sizes, obstacle placements, and start/end positions. For each configuration, it algorithmically computes the solution and generates both the task and ground-truth outputs. To ensure consistency across tasks, VBVR offers a standardized generator template that defines interfaces, output formats, and validation hooks.

Each generator deterministically produces a four-component output: (1) `first_frame.png` (initial state),

Table 3 Benchmarking results on **VBVR-Bench**. Overall In-Domain (ID) and Out-of-Domain (OOD) scores are reported alongside category-wise performance. Higher is better. **Bold**: best in group; underline: second best.

Models	In-Domain by Category							Out-of-Domain by Category					
	Overall	Avg.	Abst.	Know.	Perc.	Spat.	Trans.	Avg.	Abst.	Know.	Perc.	Spat.	Trans.
Human	0.974	0.960	0.919	0.956	1.00	0.95	1.00	0.988	1.00	1.00	0.990	1.00	0.970
Open-source Models													
CogVideoX1.5-5B-12V (Yang et al., 2024)	0.273	0.283	0.241	0.328	0.257	0.328	0.305	0.262	<u>0.281</u>	0.235	0.250	0.254	0.282
HunyuanVideo-12V (Kong et al., 2024)	0.273	0.280	0.207	0.357	0.293	0.280	<u>0.316</u>	0.265	0.175	0.369	0.290	<u>0.253</u>	0.250
Wan2.2-12V-A14B (WanTeam, 2025)	0.371	0.412	0.430	0.382	0.415	0.404	0.419	0.329	0.405	0.308	0.343	0.236	<u>0.307</u>
LTX-2 (HaCohen et al., 2026)	<u>0.313</u>	<u>0.329</u>	<u>0.316</u>	<u>0.362</u>	<u>0.326</u>	<u>0.340</u>	0.306	<u>0.297</u>	0.244	<u>0.337</u>	<u>0.317</u>	0.231	0.311
Proprietary Models													
Runway Gen-4 Turbo (Runway Research, 2025)	0.403	0.392	0.396	0.409	0.429	0.341	0.363	0.414	0.515	<u>0.429</u>	0.419	0.327	0.373
Sora 2 (OpenAI, 2025)	0.546	0.569	<u>0.602</u>	<u>0.477</u>	0.581	0.572	0.597	0.523	<u>0.546</u>	0.472	0.525	0.462	0.546
Kling 2.6 (Kuaishou Technology, 2025)	0.369	0.408	0.465	0.323	0.375	0.347	<u>0.519</u>	0.330	0.528	0.135	0.272	0.356	0.359
Veo 3.1 (Google DeepMind, 2026)	0.480	<u>0.531</u>	0.611	0.503	<u>0.520</u>	<u>0.444</u>	0.510	<u>0.429</u>	0.577	0.277	<u>0.420</u>	<u>0.441</u>	<u>0.404</u>
Data Scaling Strong Baseline													
VBVR-Wan2.2	0.685	0.760	0.724	0.750	0.782	0.745	0.833	0.610	0.768	0.572	0.547	0.618	0.615

(2) `prompt.txt` (task instruction), (3) `final_frame.png` (target state), and (4) `ground_truth.mp4` (complete solution trajectory). Components (1) and (2) constitute model inputs; components (3) and (4) provide verifiable supervision—complete reasoning paths that enable learning “how” to reason, not just “what” the answer is.

Task diversity is achieved through structured parameter spaces defined per generator. Parameters vary across task-relevant dimensions, including object count, spatial configuration, structural complexity, and difficulty level. Generators employ stratified sampling to ensure balanced coverage within each task’s parameter space. Before deployment, all generators undergo code review to verify scalability, visual quality, edge-case handling, and reproducibility under fixed random seeds. Only generators that satisfy these requirements are admitted to large-scale production.

3.3.3. Large-Scale Generation and Control

The final stage executes validated generators at scale within a distributed generation framework. VBVR generates one million training samples across 100 training tasks (10,000 per task) and 7500 test samples across 150 test tasks (50 per task). Training and test splits are constructed using disjoint random seed ranges to prevent data leakage. Quality control is fully automated during generation. Each sample is validated for the existence of a solution, visual compliance, and boundary constraints. Failed generations trigger automatic retries; persistent failures are logged for further generator refinement. System-level monitoring tracks generation statistics and validation failure rates across tasks. From the 150 approved task designs, we organize 100 tasks for training and 100 tasks for testing, with a carefully designed dual-split strategy to assess both in-distribution robustness and out-of-distribution generalization in Sec. 4.1.

The parameterized infrastructure supports continuous expansion: standardized generator templates enable community contributors to develop new tasks while automated validation ensures consistent quality. This positions VBVR as a living benchmark that evolves with the field’s understanding of video reasoning. Implementation details and generator specifications are provided in Sec. B.

4. Benchmark

In this section, we introduce the evaluation toolkit (Sec. 4.1) and assess its validity through alignment with human preferences (Sec. 4.2). We subsequently report the performance of leading video generation models (Sec. 4.3) and investigate the correlations among their reasoning capabilities (Sec. 4.4).

4.1. Evaluation Kit

To systematically assess model reasoning capabilities, VBVR-Bench employs a dual-split evaluation strategy across 100 diverse tasks. The first split contains 50 tasks that overlap with the training categories but differ in unseen parameter configurations and sample instances, providing a test of *in-domain generalization*. The second split includes the remaining 50 tasks, which are entirely novel and are designed to measure *out-of-domain generalization*. It tests whether models can solve reasoning challenges without prior exposure to similar structures, and thus whether they acquire transferable reasoning primitives rather than relying on task-specific memorization. Each task consists of five test samples, enabling statistically robust evaluation across diverse reasoning scenarios.

A key feature of VBVR-Bench is its fully **rule-based evaluation framework**, which is feasible because most test tasks have a unique, verifiable correct answer, allowing interpretable evaluation based on spatial position, color, object identity, path, or logical outcome. Moreover, geometric, physical, or deductive constraints are also considered in the scoring rubrics. Each of the 100 test tasks is paired with a dedicated evaluation rule, with scores on multiple aspects to compute a weighted, comprehensive score. Sub-criteria include spatial accuracy, trajectory correctness, temporal consistency, and logical validity.

For example, in the Task G-45: Key Door Matching (More examples are included in Sec. D), a green dot agent must first locate a color-specified key and then navigate to the matching door within a grid maze. Performance is scored across four weighted dimensions: target identification accuracy (30%), path validity (30%), path efficiency (20%), and animation quality (20%). Target identification verifies that the agent selects the correct key and door without confusing colors, path validity ensures the agent follows allowed paths without wall collisions, path efficiency compares the actual trajectory to the optimal BFS path, and animation quality checks smooth frame-by-frame movement and precise object alignment. A full score indicates perfection in all four dimensions (correct key and door selection, near-optimal pathing, and precise spatial and temporal alignment).

Overall, VBVR-Bench provides:

- **Reproducibility and Determinism.** The evaluation is fully deterministic and avoids the stochastic variability or hallucinations associated with LLM-based judgments.
- **Granular Verifiability.** Each task is decomposed into interpretable vectors, allowing precise measurement of spatial, temporal, and logical correctness, even at the pixel or object-property level.
- **Transparent Diagnosis.** By explicitly encoding reasoning constraints, the benchmark ranks models *and* reveals systematic trade-offs, capability gaps, trade-offs, and cross-domain performance trends.

4.2. Human Preference Alignment Analysis

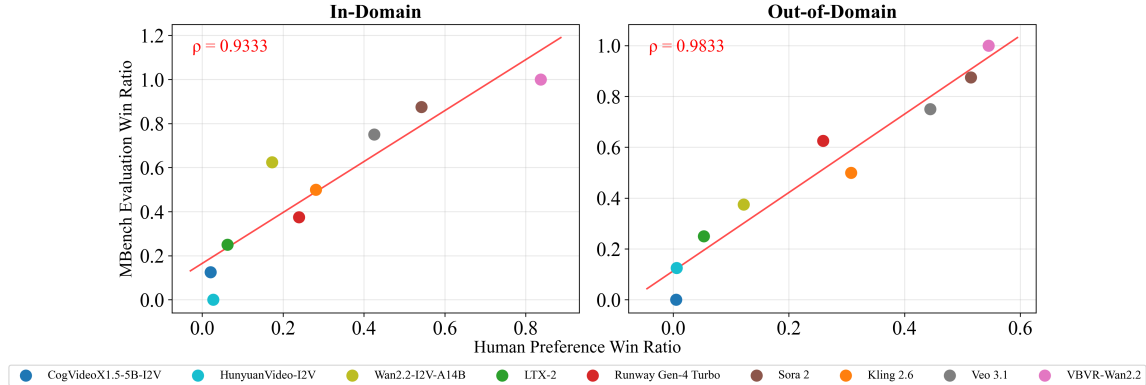
To assess alignment between VBVR-Bench and human perception, we conduct a large-scale human preference study and compare model win ratios derived from human judgments with those computed from VBVR-Bench’s automatic metrics. Specifically, human win ratios are obtained from pairwise preference annotations, where a model is considered to win if it is preferred over another model for the same prompt. In contrast, VBVR-Bench win ratios are computed by ranking models by their per-sample automatic scores and counting how often each model outperforms others. As shown in Fig. 4, the two sets of win ratios exhibit strong positive correlations across models, indicating that VBVR-Bench provides reliable and human-aligned performance estimates. Details of the study are provided in the Sec. C.2.

4.3. Leading Model Performances

Table 3 shows performance across model families. Most open-source baselines cluster between 0.27 and 0.31 overall, indicating limited capability in complex video reasoning, while Wan2.2-I2V-A14B is the strongest open-source baseline at 0.371. Proprietary models perform better overall, led by Sora 2 (0.546) and Veo 3.1 (0.480), particularly in Abstraction and Transformation categories.

Fine-tuning Wan2.2-I2V-A14B on VBVR-Dataset yields VBVR-Wan2.2, which achieves a new state of the art with an overall score of 0.685, representing an 84.6% relative improvement over its base model. VBVR-Wan2.2

Figure 4 Human alignment analysis for VBVR-Bench. Our experiments show that VBVR-Bench evaluations in all splits closely match human perceptions. In each plot, a dot represents the human preference win ratio (horizontal axis) and VBVR-Bench evaluation win ratio (vertical axis) for a particular video generation model. We linearly fit a straight line to visualize the correlation, and calculate the Spearman’s correlation coefficient (ρ) for each dimension.



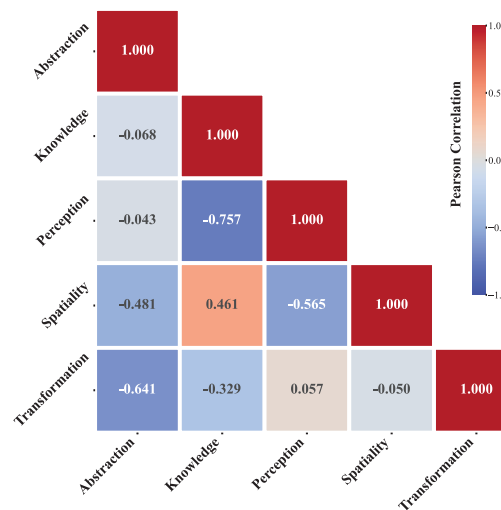
attains the best performance across all evaluated categories, with especially strong results in Spatiality and Perception, suggesting that large-scale reasoning-oriented data substantially enhances integrated world-model reasoning capabilities.

Notably, despite these gains, a considerable gap to human performance remains. This highlights the persistent challenges of long-horizon temporal reasoning and robust symbolic manipulation in video generation. We further analyze how performance evolves with increasing training data under a fixed architecture, and how in-domain and out-of-domain generalization behaviors differ, in Sec. 5.

We also analyze the stability and consistency of model behavior using domain-wise score distributions that reveal performance variability and rating noise across domains (see Sec. C.3.2).

4.4. Capability Correlation

Figure 5 Residualized capability correlation among five faculties across 9 models (Pearson ρ). We regress out a model-level general factor (overall strength) to highlight *structural* dependencies and inter-relations.



We further study *capability dependency* among the five cognitive faculties, asking whether strengths in one capability tend to co-occur with strengths in another across models. A naive correlation is often dominated by

overall model strength (i.e., stronger models score higher on *all* categories). To isolate *structural* dependencies, we compute category-level mean scores per model and regress out a model-level *general factor* (overall mean score) before measuring Pearson correlations on the residuals. See Sec. C.3.1 for more implementation details.

Figure 5 reveals non-trivial structures underlying the cognitive faculties. We observe a strong positive coupling between **Knowledge** and **Spatiality** ($\rho = 0.461$). This result is particularly interesting given the past neuroscience studies which suggest human brains use hippocampal place cells and grid cells to support concept learning. One seminal study suggests patients with bilateral hippocampal damage were impaired at learning both spatial and non-spatial configural associations in a deterministic feedback task, showing only partial, inflexible residual learning, supporting a domain-general hippocampal role in binding and configural learning (Kumaran et al., 2007). The follow-up study shows a hippocampus–ventromedial prefrontal cortex circuit supports the emergence of conceptual knowledge that guides choices, and the hippocampus is uniquely required to transfer that knowledge to a perceptually novel setting (Kumaran et al., 2009). Edward Tolman in last century hypothesizes that our spatial map of the physical world could be transferred to be used as a **cognitive map**, which is a mental representation, not only used for spatial navigation, but conceptual space construction, and general knowledge learning (Tolman, 1948; Yang et al., 2025b). Converging evidence from neuroscience and AI are coming into places to suggest the deep inter-relatedness between cognitive spatial intrinsics and knowledge acquisition (Baram et al., 2024; Whittington et al., 2025; Xiao et al., 2025).

In contrast, **Knowledge** correlates strongly negatively with **Perception** ($\rho = -0.757$). One very interesting debate in cognitive science is whether we should count core knowledge, which are knowledge that we are born with, as actually perception (Bai et al., 2025). Namely, instead of understanding intuitive physics or object permanence as a kind of knowledge, we should actually consider them as a kind of perception, which are actually supported by our perceptual neural circuits, such as medial temporal lobe, rather than our learning and memory circuits, such as hippocampus (Hassabis & Maguire, 2009; Martin & Barense, 2023)

Abstraction shows a strong negative correlation with **Transformation** ($\rho = -0.641$) and a moderate one with **Spatiality** ($\rho = -0.481$), and do not show any signs of positive correlations with any other cognitive faculties. This result is consistent with our understanding with the modularity of abstraction faculty in our brain, namely prefrontal cortex (Vaidya & Badre, 2022; Passingham & Lau, 2023; Bein & Niv, 2025; Li et al., 2026)

Moreover, **Perception** trades off with **Spatiality** ($\rho = -0.565$) but is nearly uncorrelated with both **Abstraction** ($\rho = -0.043$) and **Transformation** ($\rho = 0.057$). **Transformation** is also nearly uncorrelated with **Spatiality** ($\rho = -0.050$). Overall, VBVR-Bench not only ranks models but also enables interpretable diagnosis of how capabilities co-develop or decouple across systems.

5. VBVR-Wan2.2 Analysis

We further investigate VBVR-Wan2.2 to gain insights into scaling video reasoning. We first describe the experimental settings (Sec. 5.1), followed by an analysis of the scaling behavior (Sec. 5.2), comprehensive qualitative evaluations (Sec. 5.3), and performance on general video benchmarks (Sec. 5.4).

5.1. Experiment settings

We conduct all experiments on Wan2.2-I2V-A14B without architectural modifications, as the goal of VBVR-Wan2.2 is to **investigate data scaling behavior** and provide a **strong baseline model** for the video reasoning research community. Leveraging the VBVR-Dataset, which to our knowledge constitutes one of the largest video reasoning datasets to date, enables a systematic investigation of scaling behaviors in video-based reasoning under a fixed model architecture. For training, we adopt a learning rate of $1e-4$ and train for one epoch in each experiment. We employ LoRA adaptation on the DiT backbone, and applying LoRA to the modules q, k, v, o, ffn.0, ffn.2 with a lora rank of 32.

Table 4 Performance by Data Scale (0K–500K). **Bold**: best per column; underline: second best.

Models	Overall	In-Domain by Category						Out-of-Domain by Category					
		Avg.	Abst.	Know.	Perc.	Spat.	Trans.	Avg.	Abst.	Know.	Perc.	Spat.	Trans.
0K	0.371	0.412	0.430	0.382	0.415	0.404	0.419	0.329	0.405	0.308	0.343	0.236	0.307
50K	0.549	0.576	0.527	0.584	0.537	0.642	0.654	0.522	0.596	0.584	0.507	0.482	0.490
100K	0.623	0.701	0.622	0.680	0.777	0.719	0.759	0.545	0.622	0.524	0.533	0.557	0.517
200K	0.689	<u>0.767</u>	<u>0.739</u>	0.709	0.791	0.799	0.825	0.611	<u>0.748</u>	0.621	<u>0.545</u>	0.659	0.599
300K	0.682	0.763	0.733	0.713	0.795	<u>0.776</u>	0.827	0.601	0.732	0.596	0.542	<u>0.628</u>	<u>0.600</u>
400K	0.682	0.771	0.744	<u>0.744</u>	<u>0.793</u>	0.753	0.848	0.593	0.742	0.592	0.532	0.605	0.588
500K	<u>0.685</u>	0.760	0.724	0.750	0.782	0.745	<u>0.833</u>	<u>0.610</u>	0.768	0.572	0.547	0.618	0.615

5.2. Scaling Curve

To systematically investigate data scaling behavior, we progressively increase the training data size from 0K samples (the original Wan2.2 base model) to 500K samples (VBVR-Wan2.2), and report the corresponding performance changes in Tab. 4.

First, training VBVR-Wan2.2 shows clear but **saturation gains from data scaling**. In-domain (ID) performance improves substantially with increased training data, rising from 0.412 at initialization to about 0.771 at 400K samples, after which gains plateau and slightly fluctuate. The failure to approach perfect accuracy, even within familiar distributions, suggests that current video generation architectures exhibit fundamental representational and optimization bottlenecks. In particular, these tasks require the simultaneous satisfaction of logical constraints and long-term temporal consistency, while the stochastic nature of video generation introduces cumulative rendering noise and temporal drift. Importantly, this saturation regime makes VBVR-Dataset a valuable testbed for researchers to investigate architectural advances, such as explicit state tracking, structured reasoning modules, or self-correction mechanisms, under controlled and scalable evaluation settings.

Second, examining **generalization to out-of-domain (OOD) tasks** highlights critical insights. Both ID and OOD performance improve with more data, ID from 0.412 to 0.760, and OOD from 0.329 to 0.610. This indicates that **scaling data enhances transferable reasoning capabilities** beyond memorized patterns. Our qualitative analysis in Sec. 5.3 further illustrates how the model benefits from increased training data and generalizes to out-of-domain tasks, providing interpretable insights into improvements in temporal consistency, logical reasoning, and task transferability. However, a persistent 15% generalization gap remains, suggesting that **increasing data within fixed task distributions is insufficient for robust systematic generalization**. With our data factory, we plan to continuously introduce **new task families and richer compositional regimes** in future releases, enabling broader coverage of reasoning patterns and better closing the ID–OOD gap.

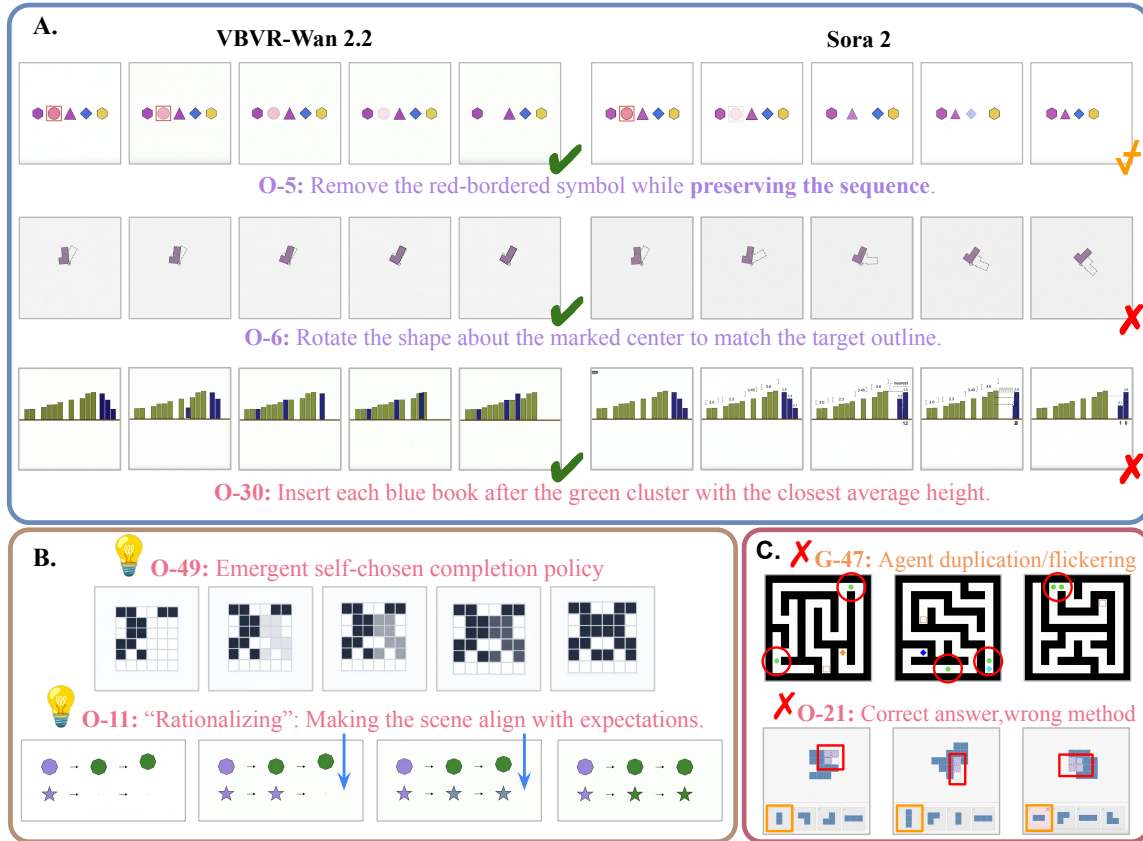
5.3. Qualitative Analysis

We qualitatively compare Wan2.2-I2V-A14B (base model), VBVR-Wan2.2, and the strongest proprietary baseline in our study, Sora 2. A recurring pattern is that, after VBVR training, VBVR-Wan2.2 can match or even surpass Sora 2 on a broad set of tasks that require *verifiable* manipulations under stable scenes. This motivates our central takeaway: **controllability before reasoning**. If a model freely rewrites the scene (background/layout/object identity) during generation, intermediate states become unreliable and any “reasoning action” (delete/move/mark) is no longer verifiable. In practice, the base model(Wan2.2-I2V-A14B) often fails in precisely this way: it may not preserve target identity or stable layouts, thereby breaking the prerequisite for manipulation-based reasoning.

To make qualitative comparisons direct and reproducible, we select examples as **same-task, same-sample comparisons** whenever multiple models are shown on the same case. Importantly, the representative cases in Fig. 6 are **out-of-domain (OOD) task families held out from training**, so improvements reflect transfer to novel task structures rather than memorization.

Controllable execution under constraints (VBVR-Wan2.2 vs Sora 2). Panel A highlights that VBVR training primarily improves *constraint-following, tool-like execution* under stable scenes. On O–5 Task, Sora 2 introduces extra, unnecessary operations: after deleting the target symbol, it further merges/re-lays the remaining symbols, violating the intended minimal-edit constraint from the task. In contrast, VBVR-Wan2.2

Figure 6 Qualitative overview on held-out OOD task families. Panel A presents same-task, same-sample comparisons between VBVR-Wan2.2 and Sora 2 on three controllable-execution tasks: O-5 (delete the marked symbol with minimal unintended changes), O-6 (apply a 2D geometric rotation under the target cue), and O-30 (rearrange a bookshelf by moving an object into the designated slot), with checkmarks/crosses indicating task success/failure. Panel B shows VBVR-Wan2.2-only emergent behaviors on O-49 (complete a symmetric pattern with a consistent self-chosen policy) and O-11 (“rationalizing”: modifying intermediate elements to fit an internally assumed transformation narrative). Panel C reports honest boundaries of VBVR-Wan2.2 on G-47 (long-horizon key-door navigation, with possible agent duplication/flickering) and O-21 (blueprint gap filling, where the video can be correct yet procedurally unfaithful).



exhibits an emergent “do exactly what is asked” capability, deleting the marked symbol *without* additional changes. On O-6 Task, Sora 2 may fail to maintain scene control and to distinguish the target region from the object to be manipulated, leading to a degenerate outcome where the box and object rotate together. In contrast, VBVR-Wan2.2 correctly separates the target cue from the manipulated object and performs a pivot-based rotation that aligns with the task requirement, suggesting emergent geometric manipulation skills beyond the training task families. On O-30, VBVR-Wan2.2 successfully performs the required constrained relocation (moving a book into the designated slot). Notably, Sora 2 can fail by producing auxiliary markings/lines without executing the actual object manipulation, illustrating that even strong proprietary models may break down when success requires precise, constraint-following control rather than generic scene editing.

Emergent strategies and multi-step behavior (VBVR-Wan2.2). Beyond controlled, tool-like execution, we observe emergent *strategy-level* regularities and multi-step behaviors on OOD task families. On O-49, VBVR-Wan2.2 often produces a rule-consistent completion of the missing half while exhibiting a distinctive, *self-chosen* completion policy: across samples, the completion typically appears as a smooth, coherent “fade-in” fill rather than discrete cell-by-cell edits. This consistency suggests that the model is not merely matching static templates, but is transferring controllable execution primitives and organizing them into a stable policy under a

new task structure. On O-11, we sometimes observe behaviors resembling “understand \rightarrow act \rightarrow adjust”. In addition to applying the intended two-step transformation to the queried shape (first change color, then move it), VBVR-Wan2.2 may modify intermediate elements (e.g., shifting a misaligned reference shape toward the arrow cue; arrows are manually overlaid for visualization), effectively *rationalizing* an internally assumed transformation narrative. While such interventions may conflict with the ground-truth reasoning trace and still yield imperfect final answers, they provide a qualitative signal that the model is maintaining scene-level coherence and executing multi-step plans rather than producing one-shot, uncontrolled scene rewrites.

Limitations and failure modes (VBVR-Wan2.2). Despite improved scene controllability, several challenging regimes remain. We observe *process unfaithfulness* in tasks with explicit procedural ground truth. On O-21 (*construction blueprint*), the gold procedure scans candidate pieces one-by-one, previews each candidate at the gap, marks incorrect candidates with a cross, and stops when the correct candidate is found and placed. The generated video can mimic a plausible-looking trial-and-error process without faithfully reflecting the true decision mechanism (“correct answer, wrong method”), highlighting the need for stronger process-level supervision and evaluation. Finally, long-horizon control can break down in interactive tasks. On G-47, compared to the base model that may move doors/keys directly, VBVR-Wan2.2 better distinguishes the agent from scene entities and exhibits the correct high-level subgoal structure (fetch key \rightarrow reach door). However, it can still suffer from control failures such as agent duplication/flickering when traversing a coherent path, indicating that maintaining identity and stable dynamics over long horizons remains an open problem.

In summary, these qualitative insights reinforce a fundamental shift in evaluating video intelligence: **controllability is the bedrock of verifiable reasoning**. Our results demonstrate that VBVR training moves beyond generic video synthesis, instilling a ‘controllability-first’ execution logic that generalizes even to novel, out-of-domain task structures. While VBVR-Wan2.2 shows a nascent ability to coordinate multi-step strategies, the remaining gap in process faithfulness and long-term identity stability highlights the next frontier. Achieving true video reasoning will require not just larger scale, but a move toward models that can maintain rigorous causal and physical constraints over extended temporal horizons.

5.4. General Performance on VBench++

Table 5 Comprehensive evaluation results on VBench-I2V.

Model	Total Score	I2V Score	Quality Score	Video-Text Camera Motion	Video-Image Subject Consist.	Video-Image Backgr. Consist.	Subject Consistency	Background Consistency	Motion Smoothness	Dynamic Degree	Aesthetic Quality	Imaging Quality
Wan2.2-I2V-A14B	0.8816	0.9582	0.8050	0.5444	0.9752	0.9903	0.9468	0.9672	0.9832	0.5285	0.6153	0.7036
VBVR-Wan2.2	0.8835	0.9678	0.7992	0.6592	0.9804	0.9921	0.9547	0.9722	0.9852	0.4106	0.6153	0.7080

To evaluate the performance of VBVR-Wan2.2 in real-world video generation scenarios, we benchmarked it against the Wan2.2-I2V-A14B base model using the VBench-I2V suite. As shown in the Tab. 5, After LoRA training on VBVR-Dataset, the model maintains a high level of performance across all core metrics, demonstrating that VBVR-Wan2.2 does not undermine the fundamental generative capabilities of the base model. Notably, we observed a significant increase in Video-Text Camera Motion Consistency (rising from 0.5444 to 0.6592), accompanied by a decrease in Dynamic Degree. These quantitative results align closely with our qualitative findings. That is, the model exhibits a more precise understanding of motion dynamics, effectively discerning which regions require temporal change and which should remain preserved. This balance results in videos that are both more stable and better aligned with the provided motion prompts.

6. Conclusion

In this work, we present VBVR-Dataset, the first large-scale and diverse training dataset designed for video reasoning, along with VBVR-Bench, a comprehensive evaluation toolkit for verifiable and reproducible assessment. Through systematic scaling studies, we demonstrate that increasing model scale leads to early signs of emergent generalization in video reasoning.

References

- Allison, H. E. *Kant's Transcendental Idealism: An Interpretation and Defense*. Yale University Press, New Haven, revised and enlarged edition, 2004.
- Andersen, R. A., Snyder, L. H., Bradley, D. C., and Xing, J. Multimodal representation of space in the posterior parietal cortex and its use in planning movements. *Annual Review of Neuroscience*, 20:303–330, 1997. doi: 10.1146/annurev.neuro.20.1.303.
- Anderson, J. R. *Rules of the Mind*. Lawrence Erlbaum Associates, Hillsdale, NJ, 1993.
- Anderson, J. R. *How Can the Human Mind Occur in the Physical Universe?* Oxford University Press, 2007.
- Anderson, J. R. *Language, memory, and thought*. Psychology Press, 2013.
- Anderson, J. R. and Lebiere, C. *The Atomic Components of Thought*. Lawrence Erlbaum Associates, Mahwah, NJ, 1998.
- Aristotle. On memory. In Barnes, J. (ed.), *The Complete Works of Aristotle: The Revised Oxford Translation*, volume 1, pp. 714–720. Princeton University Press, 1984a.
- Aristotle. Metaphysics. In Barnes, J. (ed.), *The Complete Works of Aristotle: The Revised Oxford Translation*, volume 2, pp. 1552–1728. Princeton University Press, 1984b.
- Aristotle. *Physics*, volume 1. Princeton University Press, 1984c.
- Aristotle. *Posterior Analytics*, volume 1. Princeton University Press, 1984d.
- Aristotle. Prior analytics. In Barnes, J. (ed.), *The Complete Works of Aristotle: The Revised Oxford Translation*, volume 1 of *Bollingen Series*. Princeton University Press, Princeton, NJ, 1984e.
- Aristotle. Sense and sensibilia. In Barnes, J. (ed.), *The Complete Works of Aristotle: The Revised Oxford Translation*, volume 1, pp. 693–713. Princeton University Press, 1984f.
- Aristotle. On the soul. In Barnes, J. (ed.), *The Complete Works of Aristotle: The Revised Oxford Translation*, volume 1, pp. 641–692. Princeton University Press, 1984g.
- Badre, D. and Nee, D. E. Frontal cortex and the hierarchical control of behavior. *Trends in Cognitive Sciences*, 22(2):170–188, 2018.
- Bai, D., Hafri, A., Izard, V., Firestone, C., and Strickland, B. “core perception”: Re-imagining precocious reasoning as sophisticated perceiving. *Behavioral and Brain Sciences*, pp. 1–75, 2025.
- Baillargeon, R., Spelke, E. S., and Wasserman, S. Object permanence in five-month-old infants. *Cognition*, 20(3):191–208, 1985.
- Baker, N., Lu, H., Erlikhman, G., and Kellman, P. J. Deep convolutional networks do not classify based on global object shape. *PLoS Computational Biology*, 14(12):e1006613, 2018. doi: 10.1371/journal.pcbi.1006613.
- Banino, A., Barry, C., Uria, B., Blundell, C., Lillicrap, T., Mirowski, P., Pritzel, A., Chadwick, M. J., Degris, T., Modayil, J., Wayne, G., Soyer, H., Viola, F., Zhang, B., Goroshin, R., Rabinowitz, N., Pascanu, R., Beattie, C., Petersen, S., Sadik, A., Gaffney, S., King, H., Kavukcuoglu, K., Hassabis, D., Hadsell, R., and Kumaran, D. Vector-based navigation using grid-like representations in artificial agents. *Nature*, 557(7705): 429–433, 2018. doi: 10.1038/s41586-018-0102-6.
- Bao, P., She, L., McGill, M., Bhattacharyya, R., and Tsao, D. Y. A map of object space in primate inferotemporal cortex. *Nature*, 583:103–108, 2020. doi: 10.1038/s41586-020-2350-5.

- Baram, A., Nili, H., Barreiros, I., Samborska, V., Behrens, T. E., and Garvert, M. M. An abstract relational map emerges in the human medial prefrontal cortex with consolidation. *bioRxiv*, pp. 2024–10, 2024.
- Behrens, T. E. J., Muller, T. H., Whittington, J. C. R., Mark, S., Baram, A. B., Stachenfeld, K. L., and Kurth-Nelson, Z. What is a cognitive map? Organizing knowledge for flexible behavior. *Neuron*, 100(2): 490–509, 2018. doi: 10.1016/j.neuron.2018.10.002.
- Bein, O. and Niv, Y. Schemas, reinforcement learning and the medial prefrontal cortex. *Nature Reviews Neuroscience*, 26(3):141–157, 2025.
- Bengio, Y., Courville, A., and Vincent, P. Representation learning: A review and new perspectives. *IEEE Transactions on Pattern Analysis and Machine Intelligence*, 35(8):1798–1828, 2013.
- Bertolero, M. A., Yeo, B. T. T., and D’Esposito, M. The modular and integrative functional architecture of the human brain. *Proceedings of the National Academy of Sciences*, 112(49):E6798–E6807, 2015. doi: 10.1073/pnas.1510619112.
- Bonhoeffer, T. and Grinvald, A. Iso-orientation domains in cat visual cortex are arranged in pinwheel-like patterns. *Nature*, 353:429–431, 1991.
- Bowman, C. R. and Zeithamova, D. Abstract memory representations in the ventromedial prefrontal cortex and hippocampus support concept generalization. *Journal of Neuroscience*, 38(10):2605–2614, 2018.
- Brincat, S. L., Siegel, M., von Nicolai, C., and Miller, E. K. Gradual progression from sensory to task-related processing in cerebral cortex. *Proceedings of the National Academy of Sciences*, 115(30):E7202–E7211, 2018.
- Burgess, P. W., Dumontheil, I., and Gilbert, S. J. The gateway hypothesis of rostral prefrontal cortex (area 10) function. *Trends in Cognitive Sciences*, 11(7):290–298, 2007.
- Cai, Z., Qiu, H., Ma, T., Zhao, H., Zhou, G., Huang, K.-H., Kordjamshidi, P., Zhang, M., Xiao, W., Gu, J., Peng, N., and Hu, J. MMGR: Multi-modal generative reasoning. *arXiv preprint arXiv:2512.14691*, 2025. URL <https://arxiv.org/abs/2512.14691>.
- Calvert, G. A. Crossmodal processing in the human brain: Insights from functional neuroimaging studies. *Cerebral Cortex*, 11(12):1110–1123, 2001.
- Carey, S. *The Origin of Concepts*. Oxford Series in Cognitive Development. Oxford University Press, New York, 2009.
- Carey, S. Précis of The Origin of Concepts. *Behavioral and Brain Sciences*, 34(3):113–124, 2011.
- Carey, S. and Spelke, E. Science and core knowledge. *Philosophy of Science*, 63(4):515–533, 1996.
- Chakladar, D. D. Cortex level connectivity between act-r modules during eeg-based n-back task. *Cognitive Neurodynamics*, 18(6):4033–4045, December 2024. doi: 10.1007/s11571-024-10177-y.
- Chen, H. H., Lan, D., Shu, W.-J., Liu, Q., Wang, Z., Chen, S., Cheng, W., Chen, K., Zhang, H., Zhang, Z., Guo, R., Cheng, Y., and Chen, Y.-C. Tivibench: Benchmarking think-in-video reasoning for video generative models. *arXiv preprint arXiv:2511.13704*, 2025. URL <https://arxiv.org/abs/2511.13704>.
- Christoff, K., Keramiatian, K., Gordon, A. M., Smith, R., and Mädlar, B. Prefrontal organization of cognitive control according to levels of abstraction. *Brain Research*, 1286:94–105, 2009.
- Colby, C. L. and Goldberg, M. E. Space and attention in parietal cortex. *Annual Review of Neuroscience*, 22: 319–349, 1999. doi: 10.1146/annurev.neuro.22.1.319.
- d’anthropologie de Paris, S. *Bulletins de la Société d’anthropologie de Paris*. Masson., 1898.

- DiCarlo, J. J., Zoccolan, D., and Rust, N. C. How does the brain solve visual object recognition? *Neuron*, 73(3):415–434, 2012.
- Friston, K. The free-energy principle: A unified brain theory? *Nature Reviews Neuroscience*, 11:127–138, 2010. doi: 10.1038/nrn2787.
- Geirhos, R., Narayanappa, K., Mitzkus, B., Thieringer, T., Bethge, M., Wichmann, F. A., and Brendel, W. Partial success in closing the gap between human and machine vision. *Advances in Neural Information Processing Systems*, 34:23885–23899, 2021.
- Gentner, D. Structure-mapping: A theoretical framework for analogy. *Cognitive Science*, 7(2):155–170, 1983.
- Gentner, D. and Hoyos, C. Analogy and abstraction. *Topics in Cognitive Science*, 9(3):672–693, 2017. doi: 10.1111/tops.12278.
- Ghazanfar, A. A. and Schroeder, C. E. Is neocortex essentially multisensory? *Trends in Cognitive Sciences*, 10(6):278–285, 2006. doi: 10.1016/j.tics.2006.04.008.
- Gibson, J. *The ecological approach to visual perception: classic edition*, 2014.
- Gilboa, A. and Marlatte, H. Neurobiology of schemas and schema-mediated memory. *Trends in Cognitive Sciences*, 21(8):618–631, 2017.
- Goodale, M. A. and Milner, A. D. Separate visual pathways for perception and action. *Trends in Neurosciences*, 15(1):20–25, 1992. doi: 10.1016/0166-2236(92)90344-8.
- Google DeepMind. Veo 3.1. Technical report, Google DeepMind, 2026. URL <https://blog.google/innovation-and-ai/technology/ai/veo-3-1-ingredients-to-video/>. Released January 13, 2026.
- Greco, A., Moser, J., Preissl, H., and Siegel, M. Predictive learning shapes the representational geometry of the human brain. *Nature communications*, 15(1):9670, 2024.
- Guo, Z., Chen, X., Zhang, R., An, R., Qi, Y., Jiang, D., Li, X., Zhang, M., Li, H., and Heng, P.-A. Are video models ready as zero-shot reasoners? an empirical study with the MME-CoF benchmark. *arXiv preprint arXiv:2510.26802*, 2025. URL <https://arxiv.org/abs/2510.26802>.
- Guyer, P. *Kant and the Claims of Knowledge*. Cambridge University Press, Cambridge, 1987.
- HaCohen, Y., Brazowski, B., Chiprut, N., Bitterman, Y., Kvochko, A., Berkowitz, A., Shalem, D., Lifschitz, D., Moshe, D., Porat, E., Richardson, E., Shiran, G., Chachy, I., Chetboun, J., Finkelson, M., Kupchick, M., Zabari, N., Guetta, N., Kotler, N., Bibi, O., Gordon, O., Panet, P., Benita, R., Armon, S., Kulikov, V., Inger, Y., Shiftan, Y., Melumian, Z., and Farbman, Z. Ltx-2: Efficient joint audio-visual foundation model, 2026. URL <https://arxiv.org/abs/2601.03233>. Submitted 6 Jan 2026.
- Hafting, T., Fyhn, M., Molden, S., Moser, M.-B., and Moser, E. I. Microstructure of a spatial map in the entorhinal cortex. *Nature*, 436(7052):801–806, 2005. doi: 10.1038/nature03721.
- Hassabis, D. and Maguire, E. A. The construction system of the brain. *Philosophical Transactions of the Royal Society B: Biological Sciences*, 364(1521):1263–1271, 2009.
- He, X., Fan, Z., Li, H., Zhuo, F., Xu, H., Cheng, S., Weng, D., Liu, H., Ye, C., and Wu, B. RULER-bench: Probing rule-based reasoning abilities of next-level video generation models for vision foundation intelligence. *arXiv preprint arXiv:2512.02622*, 2025. URL <https://arxiv.org/abs/2512.02622>.
- Hegarty, M., Montello, D. R., Richardson, A. E., Ishikawa, T., and Lovelace, K. Spatial abilities at different scales: Individual differences in aptitude-test performance and spatial-layout learning. *Intelligence*, 34(2):151–176, 2006. doi: 10.1016/j.intell.2005.09.005.

- Hélie, S. and Sun, R. Creative problem solving: A CLARION theory. In *2010 International Joint Conference on Neural Networks (IJCNN)*, pp. 1460–1466, Barcelona, Spain, 2010. IEEE. doi: 10.1109/IJCNN.2010.5596891. URL <https://doi.org/10.1109/IJCNN.2010.5596891>.
- Helmholtz, H. v. *Treatise on physiological optics, 3 vols.* Optical Society of America, 1924.
- Ho, J., Jain, A., and Abbeel, P. Denoising diffusion probabilistic models. In *Advances in Neural Information Processing Systems (NeurIPS)*, volume 33, pp. 6840–6851, 2020.
- Holyoak, K. J. Analogy and relational reasoning. In Holyoak, K. J. and Morrison, R. G. (eds.), *The Oxford Handbook of Thinking and Reasoning*, pp. 234–259. Oxford University Press, 2012.
- Holyoak, K. J., Gentner, D., and Kokinov, B. N. Introduction: The place of analogy in cognition. In Gentner, D., Holyoak, K. J., and Kokinov, B. N. (eds.), *The Analogical Mind: Perspectives from Cognitive Science*, pp. 1–19. MIT Press, 2001.
- Hubel, D. H. and Wiesel, T. N. Receptive fields, binocular interaction and functional architecture in the cat’s visual cortex. *The Journal of Physiology*, 160:106–154, 1962.
- Hubel, D. H. and Wiesel, T. N. Receptive fields and functional architecture of monkey striate cortex. *The Journal of Physiology*, 195(1):215–243, 1968.
- Hubel, D. H. and Wiesel, T. N. Ferrier lecture: Functional architecture of macaque monkey visual cortex. *Proceedings of the Royal Society of London. Series B, Biological Sciences*, 198(1130):1–59, 1977.
- Kant, I. *Critique of Pure Reason*. Cambridge University Press, Cambridge, 1781. The Cambridge Edition of the Works of Immanuel Kant.
- Kanwisher, N. Functional specificity in the human brain: A window into the functional architecture of the mind. *Proceedings of the National Academy of Sciences*, 107(25):11163–11170, 2010. doi: 10.1073/pnas.1005062107.
- Kanwisher, N., McDermott, J., and Chun, M. M. The fusiform face area: A module in human extrastriate cortex specialized for face perception. *Journal of Neuroscience*, 17(11):4302–4311, 1997. doi: 10.1523/JNEUROSCI.17-11-04302.1997.
- Kazemian, A., Elmoznino, E., and Bonner, M. F. Convolutional architectures are cortex-aligned de novo. *Nature Machine Intelligence*, 2025. doi: 10.1038/s42256-025-01142-3.
- Keil, F. C. *Concepts, kinds, and cognitive development*. mit Press, 1992.
- Keller, G. B. and Mrsic-Flogel, T. D. Predictive processing: A canonical cortical computation. *Neuron*, 100(2):424–435, 2018. doi: 10.1016/j.neuron.2018.10.003.
- Kersten, D., Mamassian, P., and Yuille, A. Object perception as bayesian inference. *Annual Review of Psychology*, 55:271–304, 2004. doi: 10.1146/annurev.psych.55.090902.142005.
- Kong, W., Tian, Q., Zhang, Z., Min, R., Dai, Z., Zhou, J., Xiong, J., Li, X., Wu, B., Zhang, J., et al. HunyuanVideo: A systematic framework for large video generative models. *arXiv preprint arXiv:2412.03603*, 2024.
- Kosslyn, S. M. *Image and Mind*. Harvard University Press, Cambridge, MA, 1980.
- Kosslyn, S. M. *Image and brain: The resolution of the imagery debate*. MIT press, 1996.
- Kriegeskorte, N. Deep neural networks: A new framework for modeling biological vision and brain information processing. *Annual Review of Vision Science*, 1:417–446, 2015.

- Kuaishou Technology. Kling AI launches video 2.6 model with “simultaneous audio-visual generation” capability, redefining AI video creation workflow. Press Release, December 2025. Model released December 3, 2025. Press release published December 5, 2025.
- Kumaran, D., Hassabis, D., Spiers, H. J., Vann, S. D., Vargha-Khadem, F., and Maguire, E. A. Impaired spatial and non-spatial configural learning in patients with hippocampal pathology. *Neuropsychologia*, 45(12): 2699–2711, 2007.
- Kumaran, D., Summerfield, J. J., Hassabis, D., and Maguire, E. A. Tracking the emergence of conceptual knowledge during human decision making. *Neuron*, 63(6):889–901, 2009.
- Körding, K. P., Beierholm, U., Ma, W. J., Quartz, S., Tenenbaum, J. B., and Shams, L. Causal inference in multisensory perception. *PLoS ONE*, 2(9):e943, 2007. doi: 10.1371/journal.pone.0000943.
- Laird, J. E., Rosenbloom, P. S., and Newell, A. Soar: An architecture for general intelligence. *Artificial Intelligence*, 33(1):1–64, 1987. doi: 10.1016/0004-3702(87)90050-6. URL [https://doi.org/10.1016/0004-3702\(87\)90050-6](https://doi.org/10.1016/0004-3702(87)90050-6).
- Langley, P., Laird, J. E., and Rogers, S. Cognitive architectures: Research issues and challenges. *Cognitive Systems Research*, 10(2):141–160, 2009. doi: 10.1016/j.cogsys.2006.07.004. URL <https://doi.org/10.1016/j.cogsys.2006.07.004>.
- LeCun, Y., Bengio, Y., and Hinton, G. Deep learning. *Nature*, 521(7553):436–444, 2015.
- Li, H., Chrysanthidis, N., Brincat, S. L., Rose, J., and Miller, E. K. Neural subspace reorganization reflects value-based decision making. *bioRxiv*, pp. 2026–02, 2026.
- Li, Y., Gao, Q., Zhao, T., Wang, B., Sun, H., Lyu, H., Hawkins, R. D., Vasconcelos, N., Golan, T., Luo, D., and Deng, H. Core knowledge deficits in multi-modal language models. 2025. URL <https://arxiv.org/abs/2410.10855>.
- Liu, X., Xu, Z., Li, M., Wang, K., Lee, Y. J., and Shang, Y. Can world simulators reason? Gen-ViRe: A generative visual reasoning benchmark. *arXiv preprint arXiv:2511.13853*, 2025. URL <https://arxiv.org/abs/2511.13853>.
- Longuenesse, B. *Kant and the Capacity to Judge: Sensibility and Discursivity in the Transcendental Analytic of the Critique of Pure Reason*. Princeton University Press, Princeton, 1998.
- Luo, D., Li, Y., and Deng, H. The philosophical foundations of growing ai like a child. *arXiv preprint arXiv:2502.10742*, 2025a.
- Luo, D., Wang, M., Wang, B., Zhao, T., Li, Y., and Deng, H. Machine psychophysics: Cognitive control in vision-language models. *arXiv preprint arXiv:2505.18969*, 2025b.
- Luo, Y., Zhao, X., Lin, B., Zhu, L., Tang, L., Liu, Y., Chen, Y.-C., Qian, S., Wang, X., and You, Y. V-reasonbench: Toward unified reasoning benchmark suite for video generation models. *arXiv preprint arXiv:2511.16668*, 2025c. URL <https://arxiv.org/abs/2511.16668>.
- Ma, W. J., Beck, J. M., Latham, P. E., and Pouget, A. Bayesian inference with probabilistic population codes. *Nature Neuroscience*, 9:1432–1438, 2006. doi: 10.1038/nn1790.
- Marr, D. *Vision: A Computational Investigation into the Human Representation and Processing of Visual Information*. W.H. Freeman, San Francisco, 1982.
- Martin, C. B. and Barense, M. D. Perception and memory in the ventral visual stream and medial temporal lobe. *Annual review of vision science*, 9(1):409–434, 2023.

- McClelland, J. L., McNaughton, B. L., and Lamminen, A. K. Integration of new information in memory: New insights from a complementary learning systems perspective. *Philosophical Transactions of the Royal Society B*, 375(1799):20190637, 2020.
- McCorduck, P. *Machines Who Think: A Personal Inquiry into the History and Prospects of Artificial Intelligence*. A K Peters/CRC Press, 2 edition, 2004. ISBN 9781568812052. doi: 10.1201/9780429258985.
- Milner, A. D. and Goodale, M. A. Two visual systems re-viewed. *Neuropsychologia*, 46(3):774–785, 2008.
- Mitchell, M. Artificial intelligence learns to reason, 2025.
- Moser, E. I. and Moser, M.-B. Grid cells and cortical representation. *Nature Reviews Neuroscience*, 15: 466–481, 2014. doi: 10.1038/nrn3766.
- Newell, A. You can’t play 20 questions with nature and win: Projective comments on the papers of this symposium. In Chase, W. G. (ed.), *Visual Information Processing*, pp. 283–308. Academic Press, New York, NY, 1973. ISBN 9780121701505. doi: 10.1016/B978-0-12-170150-5.50012-3. URL <https://linkinghub.elsevier.com/retrieve/pii/B9780121701505500123>. Proceedings of the Eighth Annual Carnegie Symposium on Cognition, Carnegie-Mellon University, Pittsburgh, Pennsylvania, May 19, 1972.
- Newell, A. and Simon, H. A. The logic theory machine – a complex information processing system. *IRE Transactions on Information Theory*, 2(3):61–79, 1956.
- Newell, A. and Simon, H. A. *Human Problem Solving*. Prentice-Hall, Englewood Cliffs, NJ, 1972. ISBN 0134454030.
- Newell, A., Shaw, J. C., and Simon, H. A. Report on a general problem solving program. In *IFIP congress*, volume 256, pp. 1959. Pittsburgh, PA, 1959.
- Nobel Prize Committee. The Nobel prize in physiology or medicine 2014. <https://www.nobelprize.org/prizes/medicine/2014/summary/>, 2014. Awarded to John O’Keefe, May-Britt Moser and Edvard I. Moser.
- O’Keefe, J. and Dostrovsky, J. The hippocampus as a spatial map: Preliminary evidence from unit activity in the freely-moving rat. *Brain Research*, 34(1):171–175, 1971. doi: 10.1016/0006-8993(71)90358-1.
- Olshausen, B. A. and Field, D. J. Emergence of simple-cell receptive field properties by learning a sparse code for natural images. *Nature*, 381:607–609, 1996.
- OpenAI. Sora: Openai’s text-to-video model. <https://openai.com/index/sora-is-here>, 2025. publicly released September 2025.
- Palmeri, T. J., Love, B. C., and Turner, B. M. Model-based cognitive neuroscience. *Journal of Mathematical Psychology*, 76(Pt B):59–64, February 2017. doi: 10.1016/j.jmp.2016.10.010.
- Papadopoulos, A., Sforzini, F., Egan, G., and Jamadar, S. Functional subdivisions within the human intraparietal sulcus are involved in visuospatial transformation in a non-context-dependent manner. *Human brain mapping*, 39(1):354–368, 2018.
- Passingham, R. E. and Lau, H. Do we understand the prefrontal cortex? *Brain Structure and Function*, 228(5): 1095–1105, 2023.
- Peebles, W. and Xie, S. Scalable diffusion models with transformers. In *Proceedings of the IEEE/CVF International Conference on Computer Vision (ICCV)*, pp. 4195–4205, 2023.
- Peng, W., Wang, G., Yang, T., Li, C., Xu, X., He, H., and Zhang, K. SVBench: Evaluation of video generation models on social reasoning. *arXiv preprint arXiv:2512.21507*, 2025.

- Petersen, S. E. and Sporns, O. Brain networks and cognitive architectures. *Neuron*, 88(1):207–219, Oct 2015. doi: 10.1016/j.neuron.2015.09.027.
- Plato. *Theaetetus*, volume 12. Harvard University Press, Cambridge, MA, 1921. Loeb Classical Library. Original work published ca. 369 BCE.
- Polyak, A., Zohar, A., Brown, A., Tjandra, A., Sinha, A., Lee, A., Vyas, A., Shi, B., Ma, C., Chuang, C., et al. MovieGen: A cast of media foundation models. *arXiv preprint arXiv:2410.13720*, 2024.
- Quian Quiroga, R., Boscaglia, M., Jonas, J., Rey, H. G., Yan, X., Maillard, L., Colnat-Coulbois, S., Koessler, L., and Rossion, B. Single neuron responses underlying face recognition in the human midfusiform face-selective cortex. *Nature Communications*, 14(1):5661, 2023.
- Ramnani, N. and Owen, A. M. Anterior prefrontal cortex: Insights into function from anatomy and neuroimaging. *Nature Reviews Neuroscience*, 5(3):184–194, 2004.
- Rao, R. P. N. and Ballard, D. H. Predictive coding in the visual cortex: A functional interpretation of some extra-classical receptive-field effects. *Nature Neuroscience*, 2(1):79–87, 1999. doi: 10.1038/4580.
- Rapaport, W. J. Has ai succeeded? 2026.
- Renner, A. Nous and aisthēsis: Two cognitive faculties in aristotle. *Méthexis*, 26(1):103–120, 2013. doi: 10.1163/24680974-90000616.
- Runway Research. Introducing runway gen-4: Next-generation ai models for media generation and world consistency. Runway Research, March 2025. URL <https://runwayml.com/research/introducing-runway-gen-4>. Accessed January 27, 2026.
- Russell, S. J. and Norvig, P. *Artificial Intelligence: A Modern Approach*. Pearson, Hoboken, 4th edition, 2021. ISBN 9780134610993.
- Shams, L. and Beierholm, U. R. Causal inference in perception. *Trends in Cognitive Sciences*, 14(9):425–432, 2010.
- Shepard, R. N. and Metzler, J. Mental rotation of three-dimensional objects. *Science*, 171(3972):701–703, 1971. doi: 10.1126/science.171.3972.701.
- Shields, C. *Aristotle: De Anima*. Oxford University Press, 2016.
- Spelke, E. S. Core knowledge. *American Psychologist*, 55(11):1233–1243, 2000. doi: 10.1037/0003-066X.55.11.1233.
- Spelke, E. S. and Kinzler, K. D. Core knowledge. *Developmental Science*, 10(1):89–96, 2007. doi: 10.1111/j.1467-7687.2007.00569.x.
- Sporns, O., Tononi, G., and Kötter, R. The human connectome: A structural description of the human brain. *PLoS Computational Biology*, 1(4):e42, 2005. doi: 10.1371/journal.pcbi.0010042.
- Stein, B. E. and Stanford, T. R. Multisensory integration: Current issues from the perspective of the single neuron. *Nature Reviews Neuroscience*, 9:255–266, 2008. doi: 10.1038/nrn2331.
- Swanson, L. R. The predictive processing paradigm has roots in kant. *Frontiers in Systems Neuroscience*, 10:79, 2016. doi: 10.3389/fnsys.2016.00079.
- Tanaka, K. Inferotemporal cortex and object vision. *Annual Review of Neuroscience*, 19:109–139, 1996.
- Tolman, E. C. Cognitive maps in rats and men. *Psychological Review*, 55(4):189–208, 1948. doi: 10.1037/h0061626.

- Tomov, M. S., Yagati, S., Kumar, A., Yang, W., and Gershman, S. J. Discovery of hierarchical representations for efficient planning. *PLoS Computational Biology*, 16(4):e1007594, 2020.
- Tong, J., Mou, Y., Li, H., Li, M., Yang, Y., Zhang, M., Chen, Q., et al. Thinking with video: Video generation as a promising multimodal reasoning paradigm. *arXiv preprint arXiv:2511.04570*, 2025.
- Treisman, A. M. and Gelade, G. A feature-integration theory of attention. *Cognitive Psychology*, 12(1): 97–136, 1980.
- Tsao, D. Y., Freiwald, W. A., Tootell, R. B. H., and Livingstone, M. S. A cortical region consisting entirely of face-selective cells. *Science*, 311(5761):670–674, 2006. doi: 10.1126/science.1119983.
- Tse, D., Takeuchi, T., Kakeyama, M., Kajii, Y., Okuno, H., Tohyama, C., Bito, H., and Morris, R. G. M. Schema-dependent gene activation and memory encoding in neocortex. *Science*, 333(6044):891–895, 2011.
- Vaidya, A. R. and Badre, D. Abstract task representations for inference and control. *Trends in cognitive sciences*, 26(6):484–498, 2022.
- von Helmholtz, H. *Handbuch der physiologischen Optik*. L. Voss, Leipzig, 1867.
- WanTeam. Wan: Open and advanced large-scale video generative models. *arXiv preprint arXiv:2503.20314*, 2025. URL <https://arxiv.org/abs/2503.20314>.
- Wedin, M. V. *Mind and Imagination in Aristotle*. Yale University Press, New Haven, 1988.
- Wernicke, C. *Der aphasische Symptomencomplex: Eine psychologische Studie auf anatomischer Basis*. Max Cohn und Weigert, Breslau, 1874. English translation: *The Symptom Complex of Aphasia*.
- Whitehead, A. N. and Russell, B. *Principia mathematica*, volume 2. The University Press, 1927.
- Whittington, J. C., Dorrell, W., Behrens, T. E., Ganguli, S., and El-Gaby, M. A tale of two algorithms: Structured slots explain prefrontal sequence memory and are unified with hippocampal cognitive maps. *Neuron*, 113(2):321–333, 2025.
- Whittington, J. C. R., Muller, T. H., Mark, S., Chen, G., Barry, C., Burgess, N., and Behrens, T. E. J. The Tolman-Eichenbaum machine: Unifying space and relational memory through generalization in the hippocampal formation. *Cell*, 183(5):1249–1263, 2020. doi: 10.1016/j.cell.2020.10.024.
- Wiedemer, T., Li, Y., Vicol, P., Gu, S. S., Matarese, N., Swersky, K., Kim, B., Jaini, P., and Geirhos, R. Video models are zero-shot learners and reasoners. *arXiv preprint arXiv:2509.20328*, 2025. URL <https://arxiv.org/abs/2509.20328>.
- Xiao, Z., Wang, X., Zhang, J., Ou, J., He, L., Qu, Y., Hu, X., Behrens, T. E., and Liu, Y. Human hippocampal ripples align new experiences with a grid-like schema. *Neuron*, 113(21):3661–3672, 2025.
- Yamakawa, H. The whole brain architecture approach: Accelerating the development of artificial general intelligence by referring to the brain. *Neural Networks*, 144:478–495, 2021. doi: 10.1016/j.neunet.2021.09.004. URL <https://www.sciencedirect.com/science/article/pii/S0893608021003543>.
- Yamins, D. L. K., Hong, H., Cadieu, C. F., Solomon, E. A., Seibert, D., and DiCarlo, J. J. Performance-optimized hierarchical models predict neural responses in higher visual cortex. *Proceedings of the National Academy of Sciences*, 111(23):8619–8624, 2014.
- Yang, C., Wan, H., Peng, Y., Cheng, X., Yu, Z., Zhang, J., Yu, J., Yu, X., Zheng, X., Zhou, D., and Wu, C. Reasoning via video: The first evaluation of video models’ reasoning abilities through maze-solving tasks. *arXiv preprint arXiv:2511.15065*, 2025a. URL <https://arxiv.org/abs/2511.15065>.

- Yang, J., Yang, S., Gupta, A. W., Han, R., Fei-Fei, L., and Xie, S. Thinking in space: How multimodal large language models see, remember, and recall spaces. In *Proceedings of the Computer Vision and Pattern Recognition Conference*, pp. 10632–10643, 2025b.
- Yang, Z., Teng, J., Zheng, W., Ding, M., Huang, S., Xu, J., Yang, Y., Hong, W., Zhang, X., Feng, G., et al. CogVideoX: Text-to-video diffusion models with an expert transformer. *arXiv preprint arXiv:2408.06072*, 2024.
- Zacks, J. M. Neuroimaging studies of mental rotation: A meta-analysis and review. *Journal of Cognitive Neuroscience*, 20(1):1–19, 2008.
- Zheng, Z., Peng, X., Yang, T., Shen, C., Li, S., Liu, H., Zhou, Y., Li, T., and You, Y. Open-SORA: Democratizing efficient video production for all. *arXiv preprint arXiv:2412.20404*, 2024.

A. Details of Cognitive Architecture

Does intelligence have a structure? Such discussion could date back to Aristotle, where cognition is treated not as a flat “inner theater”, i.e. in his mentor (Plato 1921, *Theaetetus* 189e–190a), but as an organization of *dunameis*, in other words, cognitive faculties. Knowing begins with *aisthêsis*, perception, where the senses receive the form of external things without their matter, i.e. seeing “redness,” not absorbing the red object (Aristotle 1984f;g, *De Anima* 2.1, 412a19–23; 2.12, 424a17–24). The perceived then gets filtered through *koinê aisthêsis*, in other words, common sense, where our judgments are supplied by core knowledge born with us, such as spatiality, intuitive physics, and logic thoughts (Carey & Spelke 1996; Carey 2009; Luo et al. 2025a; Li et al. 2025; Aristotle 1984g, *De Anima* 3.1, 425a27–b11). *Phantasia* serves as the substrate that preserves, recombines, organizes and transforms the perceptual *empeiria*, experiences, and stores them into *mnēmē*, memory (Aristotle 1984a;g, *De Anima* 3.3, 427b14–428a9, *On Memory*, 449b3–453b11). Above *empeiria* and *mnēmē* lies the *noûs*, the uniquely human faculty of understanding and abstraction, and from *empeiria*, *noûs* extracts *katholou*, universals, an arc that Aristotle foregrounds as he traces from *aisthêsis*, *phantasia*, *empeiria*, *mnēmē* to *noûs*. Essentially, the path to *katholou*, for Aristotle, is the path to knowledge and intelligent human behaviors, and therefore such is the flow of Aristotle’s cognitive architecture (Aristotle, 1984b, *Metaphysics* 1.1, 980a21–27).

German Idealism is another undertaking where human thinkers try to theorize the structure of our cognition and mind. Kant posits that the mind does not simply mirror the but actively structures the world that we perceive as it’s (Kant 1781, *CPR*, A19–A24/B33–B38; A30–A33/B45–B49). He holds that raw sensory input can only become meaningful when organized by the mind’s built-in frameworks – *sinnlichkeit*, a priori forms of intuition, i.e. space and time, and *verstand*, categories of understanding, which include understanding of numbers, of quality, modality, of causality, and of relations (Kant 1781, *CPR*, A50–A51/B74–B75; A80/B106). Between *sinnlichkeit* and *verstand* lies *einbildungskraft*, where structured perceptual mental content would be sent to for transformation and synthesis. Kant gives particular descriptions of such transformation of mental content: *sinnlichkeit* first organizes the spatiotemporal shape of representations, ordering raw data as a unified intuition in space and time, and *einbildungskraft* brings together intuitions so that they can be combined, and finally *verstand* recognizes the unified data by subsuming it under a category (Kant 1781, *CPR*, A98–A110). At the apex lies *vernunft*, which offers the ultimate abstraction of mental representations, and generate ideas such as the soul, the self as a whole, the world, the universe as a totality, and God (Allison 2004; Longuenesse 1998; Guyer 1987; Kant 1781, *CPR*, A327/B384; A642/B670; A249–A252).

Modern discussions on cognitive architecture usually combine with research in artificial intelligence and cognitive neuroscience. At the Dartmouth Workshop in 1956, where the term “artificial intelligence” is coined, Herbert Simon and Alan Newell has presented Logical Theorist, a computer program which they had claimed to be the “the first artificial intelligence program” (Newell & Simon, 1956; McCorduck, 2004). While Logical Theorist is narrow and could only prove 38 of the first 52 theorems in Russell’s philosophy textbook, it sparks the first AI boom where people try to build principled computer programs that would produce human-like intelligent behaviors (Whitehead & Russell, 1927; Russell & Norvig, 2021). The General Problem Solver has shown that human reasoning could be simulated using symbolic production systems, establishing a computational account of problem solving, while critiques argue such is only a subset of what human intelligence could do (Newell et al., 1959; Newell & Simon, 1972; Newell, 1973). Full-scale cognitive architecture models soon have flourished, including ACT-R, SOAR, and CLARION models (Anderson, 2013; Laird et al., 1987; Anderson & Lebiere, 1998; Anderson, 1993; 2007; Langley et al., 2009; Hélie & Sun, 2010).

As techniques in neuroscience have developed, a dialogue has emerged between cognitive architectures and brain architectures (Petersen & Sporns, 2015). Human brain is interestingly modular, with cognitive functions specifically implemented in particular physical anatomical locations, yet these specialized regions communicate constantly to orchestrate cognition (d’anthropologie de Paris, 1898; Wernicke, 1874; Kanwisher, 2010). Recently, cognitive neuroscientists hope to map out the structural and functional connectivity between brain areas as to understand the architectural organization underlying cognition (Sporns et al., 2005; Bertolero et al., 2015). Explicit combinations of the cognitive architecture approaches and connectomics approaches have

been carried out in research in recent years and yielded validations of some of the hypothesized architectural claims about human cognition in the human brain (Palmeri et al., 2017; Yamakawa, 2021; Chakladar, 2024).

Sitting on the shoulder of philosophy giants and combining works from cognitive architecture modeling and neuroscience, we have consolidated a cognitive architecture made of **perception, transformation, spatiality, abstraction, and knowledge**.

A.1. Perception

Perception is the the extraction of form without matter (Aristotle, 1984g, *De Anima* 2.12, 424a17–24). Helmholtz calls this as “unconscious inference” (von Helmholtz, 1867; Helmholtz, 1924). The visual system exemplifies perception’s hierarchical architecture. V1 neurons function as oriented edge detectors organized into columnar structures reflecting natural image statistics (Hubel & Wiesel, 1962; 1968; Bonhoeffer & Grinvald, 1991; Hubel & Wiesel, 1977; Olshausen & Field, 1996). Beyond V1, the ventral and dorsal streams achieve progressively invariant object recognition (Milner & Goodale, 2008; Goodale & Milner, 1992; DiCarlo et al., 2012; Tanaka, 1996), with category-selective regions like the fusiform face area emerging in inferotemporal cortex (Kanwisher et al., 1997; Tsao et al., 2006; Quian Quiroga et al., 2023), where cells collectively map a low-dimensional “object space” (Bao et al., 2020). Just as Kant has hypothesized (Swanson, 2016), the brain generates predictions about sensory input and computes prediction errors, with representational geometry shaped by environmental regularities (Rao & Ballard, 1999; Friston, 2010; Keller & Mrsic-Flogel, 2018; Greco et al., 2024; Kersten et al., 2004; Ma et al., 2006). Multimodal integration binds signals across modalities through causal inference in regions like superior temporal cortex (Ghazanfar & Schroeder, 2006; Stein & Stanford, 2008; Calvert, 2001; K rding et al., 2007; Shams & Beierholm, 2010). Marr’s tri-level framework connects biological and artificial vision (Marr, 1982): CNNs exhibit cortex-aligned representations, though they lack robust higher-level processing found in biological systems (Yamins et al., 2014; Kriegeskorte, 2015; Kazemian et al., 2025; Baker et al., 2018; Geirhos et al., 2021). Gibson’s ecological approach reminds us that perception ultimately serves action through affordances (Gibson, 2014)—connecting to Aristotle’s view that *aisth sis* serves the organism’s engagement with its environment. Perception constitutes the entry point of human cognitive architecture, a thesis from Marr and Gibson to modern deep learning (Gibson, 2014; Marr, 1982; Yamins et al., 2014; Kriegeskorte, 2015; Kazemian et al., 2025; Baker et al., 2018; Geirhos et al., 2021).

A.2. Transformation

Transformation refers to the cognitive faculty that manipulates, recombines, and synthesizes mental representations, corresponding to Aristotle’s *phantasia* and Kant’s *Einbildungskraft*. Aristotle insists that “whenever one contemplates, one necessarily at the same time contemplates in images,” positioning *phantasia* not as passive storage but as active transformation of *empeiria* into material suitable for *no s* (Aristotle 1984g, *De Anima* 3.7, 431a16–17; Wedin 1988). Kant systematizes this through his three syntheses, apprehension gathering the sensory manifold, reproduction in imagination holding representations together, and recognition subsuming the unified manifold under categories, with *Einbildungskraft* functioning productively to generate experiential structure by binding intuitions according to *Verstand* (Kant 1781, *CPR*, A98–A110; Longuenesse 1998; Allison 2004). Modern cognitive science operationalizes these insights: scientists have demonstrated that mental rotation operates analogically on quasi-spatial representations, proposing that mental images are constructed in a “visual buffer” for manipulation (Shepard & Metzler, 1971; Kosslyn, 1980; 1996). Another work has showed that focused attention binds preattentively registered features into coherent objects, a process that breaks down with parietal lesions, echoing Kant’s synthesis of apprehension (Kant 1781, *CPR*, A98–A110; Treisman & Gelade, 1980). Neuroscience suggests the posterior parietal cortex, particularly the intraparietal sulcus, as the substrate for transformation (Zacks, 2008; Papadopoulos et al., 2018), while cognitive architectures like ACT-R formalize this through an imaginal module with parietal correlates (Anderson, 2007). Transformation thus occupies the crucial intermediate position both Aristotle and Kant recognized: between raw *aisth sis* or *Sinnlichkeit* and the higher operations of *no s* or *Vernunft*.

A.3. Spatiality

For Kant, space constitutes an *a priori* form of *sinnlichkeit*—a transcendental precondition for perception itself, not something derived from experience (Kant 1781, *CPR*, A22–A24/B37–B40). This insight finds support in developmental psychology identifying spatiality as a core knowledge system: infants possess domain-specific machinery for representing places and their geometric relationships, with deep phylogenetic roots observable across species and cultures (Spelke & Kinzler, 2007; Spelke, 2000). Tolman first proposed that animals construct internal “cognitive maps” enabling flexible navigation beyond simple stimulus-response associations (Tolman, 1948). The neural substrates were later revealed: *place cells* in the hippocampus fire at specific locations (O’Keefe & Dostrovsky, 1971), while *grid cells* in the entorhinal cortex provide metric coordinates through hexagonal firing patterns (Hafting et al., 2005), which are discoveries recognized by the 2014 Nobel Prize as “a positioning system in the brain” (Moser & Moser, 2014; Nobel Prize Committee, 2014). The posterior parietal cortex complements this system by organizing sensory coordinates into motor-relevant reference frames (Colby & Goldberg, 1999; Andersen et al., 1997). Beyond representation, humans perform spatial operations such as mental rotation, where reaction times increase linearly with angular disparity (Shepard & Metzler, 1971; Hegarty et al., 2006). Computational models that are grid-cell-inspired have been proposed, but human-level performances remain challenging (Banino et al., 2018; Whittington et al., 2020; Behrens et al., 2018). Spatiality serves as a fundamental function, a prerequisite for perception, scaffold for memory, and substrate for reasoning in human cognitive architecture.

A.4. Abstraction

Abstraction represents the apex of our cognitive architecture, where embodied experiences are distilled into generalizable knowledge. For Aristotle, *noûs* extracts *katholou*, universals, from accumulated *empeiria* through selective attention to essential features (Aristotle, 1984b, *Metaphysics* 1.1, 980a21–27; Renero, 2013; Aristotle, 1984g, *De Anima* 3.4–8; Shields, 2016). Kant’s *Vernunft* similarly generates transcendental ideas extending beyond the categories of *Verstand*, though exceeding the boundaries of possible experience (Kant, 1781, *CPR*, A327/B384; A642/B670; Allison, 2004; Guyer, 1987). Contemporary accounts elaborate these mechanisms: one developmental psychology work demonstrates that abstract concepts emerge through Quinian Bootstrapping, producing representational systems with greater expressive power than core cognition, with concepts possessing causally deep “cores” (Carey, 2009; Carey, 2011; Carey, 2009; Keil, 1992). Gentner’s structure-mapping theory shows how analogical reasoning maps relational patterns across domains, with systematicity determining preferred mappings and enabling children to extract relational abstractions (Gentner, 1983; Gentner & Hoyos, 2017; Holyoak, 2012; Gentner, 1983; Gentner & Hoyos, 2017; Holyoak et al., 2001). Neuroscience reveals abstraction’s hierarchical implementation: the lateral PFC exhibits a rostral-to-caudal gradient whereby anterior regions process increasingly abstract information, with rostral PFC serving as a “gateway” for internally-generated thought (Badre & Nee, 2018; Christoff et al., 2009; Badre & Nee, 2018; Brincat et al., 2018; Burgess et al., 2007; Ramnani & Owen, 2004). Memory systems contribute through schema-guided consolidation, with hippocampus and vmPFC maintaining abstract prototype representations that support generalization (Bowman & Zeithamova, 2018; Gilboa & Marlatte, 2017; Tse et al., 2011; McClelland et al., 2020). Hierarchical abstraction might underly deep learning’s layered representations and cognitive architectures’ multiple processing levels (LeCun et al., 2015; Bengio et al., 2013; Anderson, 2007; Laird et al., 1987; Tomov et al., 2020; Luo et al., 2025b). Abstraction integrates the outputs of perception, transformation, and spatiality to achieve the *katholou*, knowledge, that Aristotle recognized as the *telos* of intelligent behavior (Aristotle, 1984d, *Posterior Analytics* 2.19, 100a3–100b5).

A.5. Knowledge

Aristotle opens the *Metaphysics* with the claim that “all human beings by nature desire to know” (Aristotle, 1984b, *Metaphysics* 980a21), and devotes the closing chapter of the *Posterior Analytics* to explaining how they do so. Knowledge begins in *aisthêsis*, sense perception, which deposits *mnêmê*, memory; repeated memories of the same kind consolidate into *empeiria*, experience; and from experience *noûs* abstracts the universal first principles that ground *epistêmê*, demonstrative knowledge (Aristotle, 1984d, *Posterior Analytics* II.19,

99b15–100b17). The progression is neither purely empirical nor purely rational: perception furnishes the material, but it is the active intellect that grasps the universal in the particular, “as when a rout has occurred in battle, first one soldier makes a stand, then another, until the original formation is restored” (Aristotle, 1984d, *Posterior Analytics* 100a12–13). For Aristotle, then, human cognition is structured from the outset by capacities that go beyond the sensory given, *noûs* does not learn first principles from experience so much as recognize them through it.

Kant radicalizes this insight. Whereas Aristotle allows that universals are latent in perception and extracted by intellect, Kant argues that the mind actively constitutes the very form of experience. “Thoughts without content are empty; intuitions without concepts are blind” (Kant, 1781, *CPR* A51/B75): knowledge requires both sensible *Anschauungen* delivered by receptivity and the *Kategorien* of *Verstand* imposed by spontaneity. The categories, substance, causality, unity, plurality, and the res, are not abstracted from experience but are its *a priori* conditions of possibility (Kant, 1781, *CPR* A80/B106; Longuenesse, 1998). The transcendental deduction establishes that these concepts must apply to any object of experience whatsoever, because it is only through their application that the manifold of intuition is synthesized into coherent representation (Kant, 1781, *CPR* B129–B169; Allison, 2004). Knowledge, for Kant, is thus never a passive reception but an active structuring: the mind brings to experience the very framework within which experience becomes intelligible.

Contemporary developmental psychology has furnished striking empirical support for this rationalist inheritance. Research on core knowledge demonstrates that human infants possess, from the earliest months of life, a set of domain-specific representational systems that structure cognition prior to and independently of explicit instruction (Spelke & Kinzler, 2007). These representations are abstract, often amodal, and operate according to principles that go well beyond what associative learning from perceptual statistics could deliver (Baillargeon et al., 1985). Carey’s account of conceptual change further shows that later, explicit knowledge is constructed not *ex nihilo* but through the enrichment, combination, and bootstrapping of these core systems, a process she terms Quinian bootstrapping (Carey, 2009).

Figure 7 Distribution of 150 visual reasoning tasks across five cognitive faculties in the VBVR-Dataset.

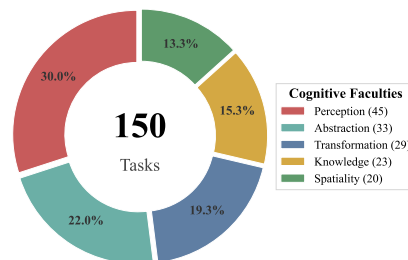


Table 6 Complete Cognitive Taxonomy of VBVR-Dataset (150 Visual Reasoning Tasks)

Task ID	Cognitive Category	Description
ABSTRACTION (33)		
G-7	Abstraction	Return objects to correct bin by category
G-26	Abstraction	Maintain object identity across different objects
G-29	Abstraction	Find extreme values in chart (with data labels)
G-37	Abstraction	Identify random symmetry patterns
G-38	Abstraction	Identify shape symmetry patterns
G-41	Abstraction	Grid highest cost path finding
G-44	Abstraction	Breadth-first search traversal
G-49	Abstraction	Complete missing contour segments
G-51	Abstraction	Predict next color in sequence
G-131	Abstraction	Select next figure in increasing size sequence
G-133	Abstraction	Select next figure in decreasing size sequence
G-134	Abstraction	Select next figure in large-small alternating sequence
G-135	Abstraction	Select next figure in small-large alternating sequence
G-193	Abstraction	Draw next sized shape in pattern
O-7	Abstraction	Shape color change operations
O-8	Abstraction	Shape rotation operations

Continued on next page

Table 6 — continued from previous page

Task ID	Cognitive Category	Description
O-9	Abstraction	Shape scaling operations
O-10	Abstraction	Shape outline fill operations
O-11	Abstraction	Shape color then move (compound operation)
O-12	Abstraction	Shape color then scale (compound operation)
O-13	Abstraction	Shape outline then move (compound operation)
O-14	Abstraction	Shape scale then outline (compound operation)
O-21	Abstraction	Construction blueprint interpretation
O-29	Abstraction	Ball color clustering and merging
O-30	Abstraction	Bookshelf organization task
O-37	Abstraction	Light sequence pattern recognition
O-43	Abstraction	Object subtraction (quantity reasoning)
O-45	Abstraction	Sequence completion task
O-47	Abstraction	Sliding puzzle solving
O-49	Abstraction	Symmetry completion task
O-54	Abstraction	Control panel symbol manipulation
O-56	Abstraction	Raven's Progressive Matrices reasoning
O-66	Abstraction	Animal color sorting task
KNOWLEDGE (23)		
G-27	Knowledge	Read chart data and semantic comprehension
G-30	Knowledge	Find extreme values in chart (without data labels)
G-35	Knowledge	Hit target after bounce
G-48	Knowledge	Multiple bounces prediction
G-160	Knowledge	Circle largest numerical value
G-162	Knowledge	Locate twelve o'clock arrows
G-163	Knowledge	Identify digits 1 and 9
G-200	Knowledge	Circle maximum value in set
G-217	Knowledge	Circle central dot
G-247	Knowledge	Identify Chinese character
G-273	Knowledge	High density liquid behavior
O-3	Knowledge	Symbol reordering operations
O-15	Knowledge	Ball bounces at given time
O-18	Knowledge	Glass refraction
O-19	Knowledge	Mirror reflection
O-23	Knowledge	Domino chain branch path prediction
O-24	Knowledge	Domino chain gap analysis
O-34	Knowledge	Dot-to-dot connection task
O-52	Knowledge	Traffic light state reasoning
O-53	Knowledge	Clock reading and time reasoning
O-62	Knowledge	Gravity physics simulation
O-75	Knowledge	Communicating vessels (fluid dynamics)
O-87	Knowledge	Fluid diffusion reasoning
PERCEPTION (45)		
G-3	Perception	Stable sort objects maintaining order
G-4	Perception	Identify and distinguish different objects
G-5	Perception	Multi-object placement to specified positions
G-9	Perception	Identify objects in specified region
G-19	Perception	Sort objects by specified rule
G-22	Perception	Attention shift to same object
G-39	Perception	Attention shift to different object
G-43	Perception	Understand scene structure and spatial layout
G-54	Perception	Connecting matching colors
G-132	Perception	Find fragment for gap filling
G-136	Perception	Locate point in overlapping area
G-137	Perception	Identify figure in overlapping area
G-138	Perception	Spot unique non-repeated color
G-141	Perception	Identify polygon with most sides
G-143	Perception	Select box with most dots
G-146	Perception	Circle all squares from mixed shapes
G-147	Perception	Identify unique figure in uniform set
G-158	Perception	Identify all hollow points
G-161	Perception	Mark second largest shape
G-165	Perception	Mark tangent point after motion
G-166	Perception	Highlight horizontal lines
G-167	Perception	Select longest polygon side
G-168	Perception	Identify rectangle nearest to square
G-169	Perception	Locate intersection of line segments
G-174	Perception	Arrange circles by circumference
G-189	Perception	Draw midpoint perpendicular line
G-195	Perception	Select nearest 2:1 rectangle
G-198	Perception	Mark right-angled triangles
G-199	Perception	Locate line intersections
G-202	Perception	Mark wave peaks

Continued on next page

Table 6 — continued from previous page

Task ID	Cognitive Category	Description
G-206	Perception	Identify pentagons
G-212	Perception	Find incorrect arrow direction
G-218	Perception	Identify largest angle in triangle
G-222	Perception	Mark tangent point of circles
G-223	Perception	Highlight horizontal lines
G-248	Perception	Mark asymmetrical shape
G-250	Perception	Color triple intersection red
O-1	Perception	Color mixing (additive)
O-2	Perception	Pigment color mixing (subtractive)
O-16	Perception	Color addition operations
O-17	Perception	Color subtraction operations
O-31	Perception	Ball eating mechanics
O-33	Perception	Counting objects accurately
O-38	Perception	Identify majority color in set
O-65	Perception	Animal size sorting
SPATIALITY (20)		
G-12	Spatiality	Grid navigation to obtain reward
G-13	Spatiality	Grid number sequence navigation
G-14	Spatiality	Grid color sequence navigation
G-15	Spatiality	Grid navigation avoiding obstacles
G-16	Spatiality	Grid navigation going through blocks
G-17	Spatiality	Grid navigation avoiding red blocks
G-18	Spatiality	Grid shortest path finding
G-31	Spatiality	Directed graph navigation
G-32	Spatiality	Undirected graph navigation
G-33	Spatiality	Visual Jenga game
G-45	Spatiality	Key-door matching puzzle
G-46	Spatiality	Find keys and open doors
G-47	Spatiality	Multiple keys for one door puzzle
G-140	Spatiality	Locate topmost unobscured figure
G-219	Spatiality	Select leftmost shape
G-221	Spatiality	Outline innermost square
O-25	Spatiality	LEGO construction assembly
O-39	Spatiality	Maze navigation and solving
O-55	Spatiality	Rotation operations
O-83	Spatiality	Planar warp verification
TRANSFORMATION (29)		
G-1	Transformation	Predict object trajectory
G-2	Transformation	Reorder objects by rule
G-6	Transformation	Resize object
G-8	Transformation	Track object movement
G-11	Transformation	Handle object reappearance after disappearance
G-21	Transformation	Multiple occlusions (vertical)
G-24	Transformation	Separate objects (no rotation)
G-25	Transformation	Separate rotating objects
G-34	Transformation	Object packing optimization
G-36	Transformation	Multiple occlusions (horizontal)
G-40	Transformation	Combined rotating objects
G-50	Transformation	Suppress spurious edges
G-194	Transformation	Construct concentric ring
G-240	Transformation	Add borders to unbordered shapes
O-4	Transformation	Symbol substitution operations
O-5	Transformation	Symbol deletion operations
O-6	Transformation	2D geometric transformation
O-22	Transformation	Construction stack (gravity balance)
O-27	Transformation	Move 2 objects to 2 targets
O-32	Transformation	Rolling ball physics
O-36	Transformation	Grid shift operations
O-44	Transformation	Rotation puzzle
O-46	Transformation	Shape sorter classification
O-58	Transformation	Symbol delete operations
O-59	Transformation	Symbol insert operations
O-60	Transformation	Symbol substitute operations
O-61	Transformation	Symbol edit operations
O-64	Transformation	Animal matching task
O-85	Transformation	2D object rotation

B. Data Curation

This appendix provides a comprehensive account of the data curation pipeline that underlies the VBVR-Bench. We detail the five-stage process from task design to benchmark construction, the quality assurance mechanisms, and the infrastructure that enables large-scale data generation.

B.1. Overview of Data Curation Pipeline

The VBVR-Bench is built through a systematic five-stage pipeline that transforms cognitive task concepts into a standardized evaluation framework.

Pipeline Flow. The data curation pipeline consists of five sequential stages. **Stage 1: Task Design** We begin by designing cognitive reasoning tasks grounded in cognitive science principles. Starting from over 300 task candidates, we employ a dual-review process to select tasks that meet six quality criteria. This stage produces two distinct task sets: 100 training tasks and 100 testing tasks with an overlapping of 50 tasks. **Stage 2: Task Implementation** Each training task is implemented as a parameterized generator capable of producing diverse samples. These generators form the our data spring, VBVR-DataFactory, a set of modular synthesis engines. All generators inherit from a standardized `BaseGenerator` template and are managed as independent repositories within a GitHub Organization. Implementation undergoes rigorous quality control by dedicated reviewers who verify scalability, code quality, and adherence to file specifications. **Stage 3: Large-Scale Distributed Generation.** The VBVR-DataFactory infrastructure orchestrates parallel generation of one million training samples (10,000 per task) stored privately on AWS S3. Simultaneously, we generate 500 fresh test cases (5 per task) from the Test task set. Each sample comprises an initial frame, task prompt, ground-truth solution, and reference video. **Stage 4: Model Evaluation.** We employ VBVR-EvalKit to evaluate eight state-of-the-art image-to-video (I2V) models on the 500 test cases, producing 4,000 generated videos. Human annotators assess each video across three reasoning-specific dimensions: Task Completion, Reasoning Logic, and Visual Quality, each scored on a 1-5 scale. **Stage 5: Benchmark Construction and Model Training.** The evaluation data is integrated into a standardized benchmark dataset. We train the VBVR-Wan on the one million training samples, demonstrating that explicit reasoning supervision significantly improves performance on reasoning-intensive tasks.

B.1.1. Key Statistics

Table 7 summarizes the scale and coverage of the VBVR benchmark:

Table 7 Data Construction Statistics

Component	Scale	Description
Task Candidates	300+	Initial task pool
Training Tasks	100	Generate training data
Test Tasks	100	50 In-Domain + 50 Out-of-Distribution
Training Samples	1,000,000	100 tasks × 10,000 samples per task
Test Cases	7,500	150 tasks × 50 samples per task
Cognitive Categories	5	Systematic coverage
Evaluated Models	8	State-of-the-art I2V models, 4 open-source, 4 commercial
Generated Videos	4,000	8 models × 500 cases
Evaluation Records	4,000	Task Completion/Reasoning Logic/Visual Quality annotations
Development Team	75	53 OSS coders + 7 full-time employees + 5 QC reviewers
Code Repositories	300+	Github Organization

B.1.2. Design Principles

The pipeline is guided by the following core design principles: **1. Dual Generalization Testing.** The In-Domain/OOD split enables evaluation of both in-task generalization (seen task types with unseen samples) and cross-task generalization (unseen task types). **2. Reasoning-First Paradigm.** Unlike benchmarks that primarily assess generation quality, VBVR emphasizes reasoning correctness through TC, RL, and VQ metrics that capture task completion, logical consistency, and visual fidelity. **3. Industrial-Scale Quality Assurance** We employ a dual-review mechanism: peer review for task design (by five task designers) and dedicated

quality control for implementation (by more than two specialized reviewers). Six quality criteria ensure tasks are well-specified, visually clear, and scalable. **4. Extensible Infrastructure.** The modular generator architecture and comprehensive evaluation toolkit facilitate easy extension with new tasks and models. **5. Cognitive Inspiration.** Our task design began with a loose cognitive taxonomy inspired by cognitive science literature. However, rather than rigidly adhering to a fixed theoretical framework, we adopted a task-driven design philosophy: we prioritized designing intellectually meaningful reasoning tasks first, then organized them into our categories. **6. Diversity Focus.** This approach contrasts with top-down frameworks that first define strict categories, then fill them with tasks. Our bottom-up approach ensured that each task possesses genuine reasoning value, and maximizing our diversity, rather than forcing tasks to fit narrow pre-determined boxes.

B.1.3. Task Selection and Filtering

Initial Pool We designed over 300 task candidates through iterative brainstorming sessions. Each designer independently proposed tasks, which were then collectively discussed and refined.

Selection Criteria (Six Standards) Tasks were evaluated against six criteria during peer review:

1. **Information Sufficiency:** The first frame must contain all information necessary for reasoning, without requiring external context.
 - ✓ Pass Example: G-15 (Grid Avoid Obstacles) — the first frame shows start point, end point, and all obstacles.
 - × Fail Example: Tasks where the goal object is initially occluded or requires additional verbal explanation.
2. **Deterministic Solution:** Tasks should have a clear, unique solution (or explicitly defined criteria for multiple valid solutions, e.g., “shortest path”).
 - ✓ Pass Example: G-18 (Grid Shortest Path) — the optimal path is unambiguous.
 - × Fail Example: Open-ended tasks with ambiguous success conditions.
3. **Video-Based Reasoning:** Tasks must be suitable for video generation models, encompassing diverse reasoning types (temporal dynamics, static recognition, logical inference).
 - ✓ Pass Example: O-23 (Domino Chain) — requires temporal causality reasoning.
 - ! Note: Unlike some benchmarks, we do NOT exclude static recognition tasks; we include both dynamic and static reasoning.
4. **Visual Clarity:** Objects must be distinguishable, text/numbers legible, and layouts uncluttered to avoid perceptual ambiguity.
5. **Parametric Diversity (Scalability):** The parameter space must be large enough to generate 10,000 non-trivial, distinct samples per task.
6. **Technical Feasibility:** Tasks must be implementable with our rendering pipeline (PIL-based), output standard file formats, and avoid edge cases (e.g., initial occlusions, boundary overflow).

Rejection Cases Here are some of the tasks were excluded:

- **A. Multi-Step Logic Chains**
 - Example: Logic Gate Circuits
 - Reason: Reasoning chains too long to clearly visualize in video format.
- **B. Complex Physics Requiring Precise Numerical Solutions**

- Example: Elastic Collisions with friction coefficients
 - Reason: Continuous parameters yield no deterministic solution (tiny parameter variations lead to drastically different trajectories); I2V models cannot precisely simulate physics.
- **C. Excessively Difficult Tasks**
 - Example: Sudoku
 - Reason: High difficulty even for humans; unsuitable for video format (better suited for static reasoning); evaluation criteria too strict (any single cell error constitutes failure).

B.1.4. Peer Review Process

All task designs underwent a structured peer review by the five task designers, with each designer evaluating others' proposals using a standardized checklist derived from the six quality criteria; tasks typically progressed through 2–3 rounds of iterative refinement based on this feedback, during which common issues were identified, including **ambiguous success conditions**, **insufficient visual clarity**, **parameter spaces too small to support 10k samples**, and **unintentional edge cases** (e.g., objects overlapping at initialization). A task advanced to implementation (Stage 2) only after receiving consensus approval from at least three reviewers. This process ensured that every task in VBVR meets rigorous cognitive and technical standards, forming a solid foundation for the subsequent implementation and evaluation stages.

B.2. Details of Task Implementation

This section details the implementation of the 200 tasks as parameterized generators. We describe the standardized architecture, code management infrastructure, parameterization strategies, visual rendering pipeline, and dedicated quality control procedures.

B.2.1. Generator Architecture and Standardization

BaseGenerator Template All task generators inherit from a standardized `BaseGenerator` abstract base class, ensuring consistent interfaces and output formats. The template defines:

1. Required Methods:

- `__init__(self, seed, params)`: Initialize generator with random seed and task-specific parameters.
- `generate_sample(self) -> Sample`: Generate a single task instance.
- `validate_sample(self, sample) -> bool`: Verify sample meets quality criteria.
- `save_sample(self, sample, output_dir)`: Save sample to standardized file structure.

2. Standard Output Format: Each sample is saved as a directory containing:

- `first_frame.png`: Initial state image (required)
- `prompt.txt`: Task instruction in natural language (required)
- `final_frame.png` or `goal.txt`: Target state or goal description
- `ground_truth.mp4`: Reference solution video demonstrating the correct reasoning process

3. Configuration Management: Generators expose configurable parameters through a `config.yaml` file specifying:

- Parameter ranges (e.g., grid size: 5-10, number of objects: 3-8)
- Difficulty levels (easy/medium/hard)
- Visual settings (resolution: 512×512, frame rate: 24 fps)

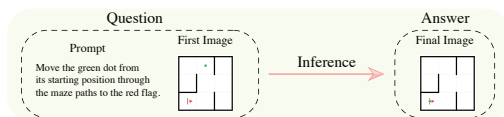
Design Rationale. The `BaseGenerator` template serves three core purposes: **Consistency**, by providing uniform interfaces that simplify integration with `VBVR-DataFactory` for batch generation; **Quality Assurance**, through the `validate_sample()` method, which enforces critical checks such as ensuring no object occlusions and that valid solutions exist; and **Extensibility**, enabling new tasks to be added by implementing the abstract methods while leveraging shared utility functions.

B.2.2. Code Management Infrastructure

All task generators are managed as independent repositories within a GitHub Organization, an architecture that provides clear organizational and operational advantages: each repository follows a strict Naming Convention of `{Type}-{ID}_{task_name}_data-generator` (e.g., `G-3_stable_sort_data-generator` and `O-15_ball_bounces_given_time_data-generator`), where `Type` denotes `G`, which are contributed by commercial enterprises, or `O`, which are contributed by OSS developers, and `ID` is a unique numeric identifier; this structure enables Independent Versioning, as each task maintains its own commit history, tags, and release cycles, and supports Modular Updates, ensuring that bug fixes or parameter adjustments to one task do not affect others.

All generators share the `core/` directory structure through Git submodules or package dependencies, ensuring consistent utility functions while allowing each task to evolve independently. This design yields several version control benefits: 1. Traceability, as each sample records the exact generator version (git commit hash) used for generation; 2. Reproducibility, enabling researchers to check out specific generator versions to reproduce sample generation; and 3. Collaboration, allowing multiple team members to work on different tasks simultaneously without merge conflicts.

Figure 8 This is a typical example of data samples in our dataset. The model receives a prompt and a first image, and is asked to generate a video that solves the prompt. Final image and ground truth videos are provided as references in data samples.



B.2.3. Parameterization Strategy for Diversity

To generate 10,000 distinct, non-trivial samples per task, we employ systematic parameterization strategies:

Example 1: G-15 (Grid Avoid Obstacles)

```
Parameters:
- grid_size: [5, 6, 7, 8, 9, 10]           # 6 options
- num_obstacles: [3, 4, 5, ..., 15]       # 13 options
- start_position: grid-dependent          # ~grid_size^2 options
- end_position: grid-dependent            # ~grid_size^2 options
- obstacle_layout: random_valid           # ~10^6 variations
```

Estimated unique samples: $> 10^9$

Sampling strategy: Constrained random sampling ensuring solvability

Example 2: O-56 (Raven's Progressive Matrices)

```
Parameters:
- pattern_type: [size_progression, rotation, color_change,
                 shape_replacement, combination]     # 5 types
- num_objects: [1, 2, 3, ..., n]                     # n options
- object_shapes: [circle, square, triangle, ...]     # 8 shapes
```

```
- progression_complexity: [simple, compound]           # 2 levels
- visual_style: [minimal, decorated]                 # 2 styles
```

Estimated unique samples: $> 10^5$

Sampling strategy: Balanced distribution across pattern types

Example 3: G-3 (Stable Sort)

Parameters:

```
- num_shape_types: [2, 3, 4]                         # 3 options
- shapes_per_type: [2, 3, 4]                         # 3 options
- color_palette: [vibrant, pastel, ...]              # 5 palettes
- initial_layout: random_permutation                 # n! permutations
- shape_geometry: [geometric, organic]               # 2 styles
```

Estimated unique samples: $> 10^6$

Sampling strategy: Uniform sampling across difficulty levels

Diversity is enforced through four complementary mechanisms: stratified sampling, which divides the parameter space into strata (e.g., difficulty levels) and samples proportionally from each; constraint satisfaction, which ensures that all generated samples are valid (e.g., mazes admit solutions and puzzles are solvable); duplicate detection, which tracks parameter combinations via hash functions to prevent exact duplicates; and visual variety, which randomizes visual attributes such as colors, sizes, and positions beyond the core reasoning parameters.

Each generated sample undergoes automatic validation, including a solvability check to verify that a ground-truth solution exists (e.g., via A* search for navigation tasks), a visual clarity check to ensure that objects do not overlap excessively and that text remains legible with a minimum font size, and a parameter bounds check to confirm that all parameters fall within their specified ranges.

B.2.4. Visual Rendering Pipeline

All visuals adhere to fixed specifications: a resolution of 512×512 pixels, 24-bit RGB color depth (8 bits per channel), a frame rate of 24 fps for ground-truth videos, and H.264 as the video codec.

B.3. Large-Scale Distributed Generation of Training Data

The VBVR-DataFactory component orchestrates the parallel generation of one million training samples using the 300+ generators in our data spring. It provides a complete, production-grade serverless system for cloud infrastructure, generation workflow, data organization, and quality assurance, enabling efficient, reliable, and cost-effective large-scale data production.

All generated samples are stored on Amazon Web Services (AWS) Simple Storage Service (S3). S3 is chosen for its ability to scale to petabyte-level data with automatic capacity management, its high durability through redundant storage across multiple availability zones, and its fine-grained access control through IAM policies. Training data are kept in private buckets with server-side encryption to prevent public exposure and test-set contamination. In addition, S3's tiered storage model makes long-term archival cost-effective.

To efficiently generate one million samples, VBVR-DataFactory employs distributed serverless processing via AWS Lambda. The system distributes tasks across up to 990 concurrent Lambda function instances, each configured with 3 GB memory and a 15-minute execution timeout. Generation tasks are queued in Amazon SQS and automatically trigger Lambda invocations, eliminating the need for manual cluster management. Within each task, samples are produced in configurable batches of 25–100 to balance memory usage and processing efficiency. A typical one-million-sample generation completes in approximately 2–4 hours with the full fleet of 990 concurrent workers, at a total cost of roughly \$800–1200 per run (primarily Lambda compute

and S3 storage). Fault tolerance is built in through SQS's automatic retry mechanism with configurable visibility timeouts, a Dead Letter Queue (DLQ) for failed messages after one retry attempt, and CloudWatch metrics for real-time monitoring of task success rates and processing durations.

The end-to-end generation pipeline begins with configuration and planning, where generators, sample counts, random seeds, and output formats are defined. Tasks are submitted to the SQS queue as Pydantic-validated JSON messages, each specifying the generator type, number of samples, starting index for global sample numbering, random seed, and output format (individual files or compressed tar archives). Lambda functions receive these messages, execute the corresponding generator subprocess, validate and rename outputs with zero-padded global indices, upload results to S3 with structured prefixes, and emit success metrics to CloudWatch. Failed tasks automatically move to the DLQ for manual inspection and resubmission after debugging.

On a per-task basis (100 samples, typical batch size), sample generation requires approximately 15 minutes, with generation speed varying significantly by task complexity—simple geometric tasks average 1–3 seconds per sample, while complex graph or physics tasks require 9–15 seconds per sample. File organization and S3 upload add 1–2 minutes depending on file sizes, and Lambda cold starts contribute an additional 5–10 seconds for the first invocation. Each task therefore completes in roughly 15–20 minutes on a Lambda instance, enabling the entire one-million-sample corpus to be produced in 2–4 hours with 990 parallel workers. For efficient access during training, VBVR-DataFactory maintains a hierarchical S3 structure organized by generator and task, with each sample directory containing standardized files (first_frame.png, prompt.txt, and optionally final_frame.png and ground_truth.mp4). This organization allows training pipelines to locate, filter, and stream data efficiently at scale through S3's prefix-based listing and parallel download capabilities.

Quality assurance is integrated throughout generation. Every sample is validated by the generator's internal checks before being saved, ensuring solvability, visual clarity, and file integrity. The system continuously monitors task success rates, processing durations, and samples uploaded through CloudWatch metrics, with alarms configured to detect anomalies such as high failure rates or DLQ accumulation. Sample diversity is enforced through unique per-task random seeds that increment deterministically across batches, preventing duplicate generation. The DLQ captures and preserves failed tasks for post-mortem analysis, enabling systematic debugging of generator issues and infrastructure failures. Across typical production runs, task validation failures occur in fewer than 1 percent of cases, primarily due to edge-case parameter combinations that are caught by Pydantic schema validation before reaching the generator. Infrastructure-related failures (timeouts, out-of-memory errors) occur in approximately 0.1–0.5 percent of tasks and are resolved through DLQ resubmission after adjusting batch sizes or addressing generator bugs.

All training samples are stored in private S3 buckets with server-side encryption (SSE-S3), versioning disabled to reduce costs, and IAM role-based access control restricted to authorized Lambda functions and training pipelines. Full S3 access logging is enabled for audit trails. The data contain no personally identifiable information, as all samples are fully synthetic and procedurally generated. Together, these design choices demonstrate that, with proper serverless engineering, million-scale, high-quality data generation is achievable, reliable, and cost-effective. The resulting one million samples form the training foundation for VBVR-Wan and future video reasoning systems.

C. VBVR-Bench Details

C.1. Model Inference Infrastructure

VBVR-Bench is an end-to-end evaluation framework that integrates large-scale model inference (or API-based invocation for proprietary models) with a rule-based evaluation engine over a standardized 100-task video reasoning benchmark. At the model level, VBVR-Bench provides a unified `VideoGenerator` abstraction that encapsulates 29 video generation systems, including closed-source models such as Google Veo, OpenAI Sora, and Runway Gen-4, as well as open-source and research models such as CogVideoX, Wan2.2, LTX-2, and HunyuanVideo. This abstraction ensures that all models are executed through an identical pipeline, eliminating confounding factors introduced by model-specific inference logic. It supports batch execution at scale, incorporates caching mechanisms to avoid redundant generations, and is fully reusable, allowing interrupted evaluations to continue without loss of progress.

C.1.1. Model Selection and Configuration

For the VBVR benchmark, we evaluate eight state-of-the-art image-to-video (I2V) models representing diverse architectures and capabilities:

Table 8 Evaluated Models

Model	Developer	Architecture	Parameters	Key Features
CogVideoX1.5-5B-I2V	Tsinghua University / Zhipu AI	Transformer-based diffusion model	5 billion	Strong text-image alignment
Wan2.2-I2V-A14B	Wanx AI	Latent diffusion with attention mechanisms	14 billion	High-fidelity temporal consistency
LTX-2	Lightricks	Efficient transformer architecture	~3 billion	Fast inference
HunyuanVideo-I2V	Tencent Hunyuan	Multi-stage diffusion with spatial-temporal attention	~7 billion	Strong on complex scenes
Veo	Google DeepMind	Proprietary (closed-source)	Unknown (large-scale)	Strong physics understanding
Sora	OpenAI	Proprietary (closed-source, rumored diffusion transformer)	Unknown (likely >10B)	Temporal coherence, realistic physics
Runway Gen-3	Runway ML	Proprietary (closed-source)	Unknown	Creative generation, text adherence
Kling 2.6	Kuaishou Technology	Proprietary (closed-source, likely diffusion-based)	Unknown	Fast inference

The models included in the benchmark are chosen to reflect the breadth and maturity of the current image-to-video landscape. The set intentionally mixes open-source and closed-source systems, ensuring that both academic and industrial approaches are represented. It spans a wide range of architectural paradigms, capturing fundamentally different design philosophies in video generation. The selected models cover a broad scale spectrum, from approximately 3B parameters to 14B+ and beyond, enabling analysis of how reasoning capability correlates with model size. All included systems represent state-of-the-art performance as of late 2025 and early 2026, ensuring that the benchmark reflects the current frontier of the field.

To ensure fair and controlled comparison, all generated videos follow the resolution of their corresponding ground-truth videos, which include both square and rectangular aspect ratios. For open-source models that support custom input resolutions, we specify the resolution to match the ground truth. For closed-source models with fixed resolution constraints (e.g., Sora 2 only supports 1280×720 or 720×1280), we pad the first-frame image with a background color and automatically detect and remove the padding during evaluation. Frame rates range from 15–24 fps depending on model requirements. For API-based models, we adopt the default or provider-recommended generation settings, while for open-source models we use the configurations reported in their original papers. This standardization removes confounding factors arising from resolution or tuning differences, ensuring that observed performance differences reflect reasoning ability rather than generation format.

C.2. Details of Human Preference Analysis

C.2.1. Data Preparation

To mitigate potential biases in pairwise comparisons, we adopt two complementary scoring schemes: **relative scoring** based on pairwise preference judgments, and **absolute scoring** based on independent per-video ratings. In cases where the absolute scores clearly indicate that one video is superior but the corresponding relative annotation contradicts this assessment, the final decision is revised in favor of the absolute judgment. For each sample consisting of a text prompt and an initial image pair p_i , we generate videos using nine

video generation models $\mathcal{M} = \{M_1, M_2, M_3, M_4, M_5, M_6, M_7, M_8, M_9\}$, producing a set of outputs $G_i = \{V_{i,1}, V_{i,2}, V_{i,3}, V_{i,4}, V_{i,5}, V_{i,6}, V_{i,7}, V_{i,8}, V_{i,9}\}$.

For relative evaluation, all pairwise combinations are constructed within each group, resulting in $\binom{9}{2} = 36$ unique video pairs per sample. For absolute evaluation, the dataset contains 500 distinct prompt–image pairs p_i . Each pair is processed by all nine models, yielding a total of $500 \times 9 = 4,500$ single-video annotation instances.

Each video is presented together with its corresponding text prompt and task-specific evaluation documents. To reduce annotation noise, every video is independently annotated five times. All samples are randomly shuffled before assigned to annotators.

C.2.2. Human annotation

Annotators are between 20 and 35 years old and possess basic domain knowledge relevant to the tasks. All annotators undergo standardized training to ensure consistent interpretation of evaluation criteria.

For relative scoring, annotators are shown two videos generated from the same prompt and are asked to select which one better completes the task and aligns with the given prompt overall, with ties allowed.

For absolute scoring, annotators rate each video along three dimensions using a 5-point Likert scale, where higher scores indicate better performance. **Task Completion (TC)** assessing whether the task goal is achieved; **Reasoning Logic (RL)**, assessing the correctness of the reasoning process; and **Visual Quality (VQ)**, assessing visual clarity, temporal coherence, and rendering fidelity.

C.2.3. Win Ratio Calculation

From relative human annotations, we compute a win ratio for each model. In each comparison, the preferred model receives a score of 1 and the other 0; in the case of a tie, both receive 0.5. Win ratios are aggregated across all pairwise comparisons for each evaluation split.

From absolute annotations, we average the scores of the TC, RL and VQ dimensions to obtain a final score per sample. These absolute scores are used for cross-verification of pairwise results and for resolving contradictory annotations between the two scoring schemes.

Finally, we compare the win ratios derived from relative human annotations (with cross-verification using absolute scores) with the win ratios computed from VBVR-Bench’s automatic evaluation metrics, and measure the correlation between the two across models.

C.3. Detailed Analysis Protocols and Additional Results

C.3.1. Residualized Capability Correlation

This section details the computation behind Fig. 5 in the main paper. Our goal is to quantify *capability dependency* between cognitive categories while avoiding trivial correlations induced by overall model strength.

Category scores. Let m index models and c index categories (five total). For each model m and category c , we compute a category-level score by averaging the per-sample Overall ratings:

$$S_{m,c} = \text{mean}(\text{Overall}) \quad \text{over all evaluated samples with Category} = c \text{ for model } m.$$

General factor. We define a model-level general factor as the overall mean score across all samples:

$$G_m = \text{mean}(\text{Overall}) \quad \text{over all evaluated samples for model } m.$$

Residualization. For each category c , we regress $S_{m,c}$ on G_m across models:

$$S_{m,c} = a_c + b_c G_m + \epsilon_{m,c},$$

and retain the residuals $\epsilon_{m,c}$ as the *strength beyond overall model quality*.

Capability dependency matrix. For each pair of categories (c_1, c_2) , we compute Pearson correlation across models using residuals:

$$R_{c_1, c_2} = \text{corr}(\{\epsilon_{m, c_1}\}_m, \{\epsilon_{m, c_2}\}_m).$$

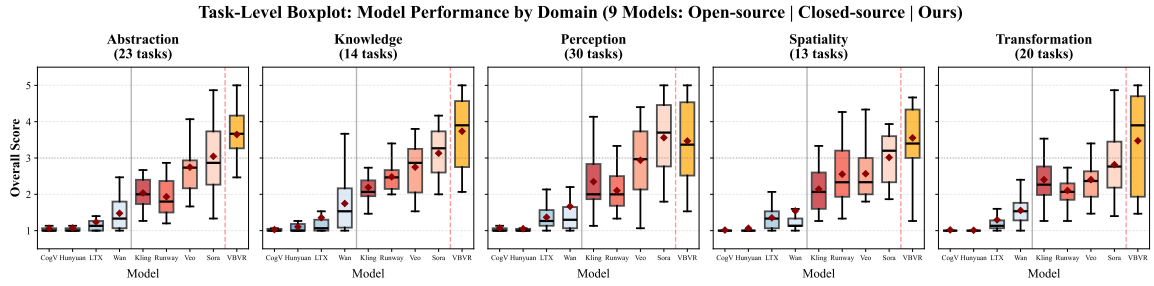
The resulting 5×5 matrix R is visualized as a heatmap (main paper, Fig. 5).

Implementation notes. We use the benchmark table and compute (i) $S_{m, c}$, (ii) G_m , (iii) residuals by ordinary least squares, and (iv) Pearson correlations on residuals. We also report Spearman ρ in auxiliary analysis to confirm robustness to monotonic transformations.

C.3.2. Domain-wise Score Distributions (Boxplots)

To complement mean performance summaries, we report domain-wise score distributions across models using boxplots: **task-level** distributions, where each point corresponds to a task mean score within a domain (capturing cross-task variability).

Figure 9 Domain-wise score distributions across 9 models (red dashed line separates baselines and VBVR-Wan2.2).



D. Selected Tasks and Rubrics

This appendix includes a curated set of tasks that require multi-step planning and/or multiple interacting constraints. For each task, we show the initial and final frames, followed by the evaluation rubric used to score model outputs.

Stable Sort (Task G-3) Rearrange objects by grouping them by shape type and sorting each group by size while preserving all attributes, testing multi-constraint spatial reasoning, attribute fidelity, and rule following.

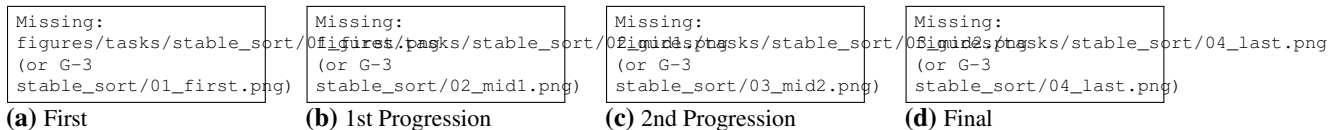


Figure 10 Stable Sort

Example Prompt “The scene contains two types of shapes, each type has three shapes of different sizes arranged randomly. Keep all shapes unchanged in appearance (type, size, and color). Only rearrange their positions: first group the shapes by type, then within each group, sort the shapes from smallest to largest (left to right), and arrange all shapes in a single horizontal line from left to right.”

Human Annotation Scoring (1–5):

- **5 (Perfect).** Correct grouping; correct within-group ascending size order (left to right); horizontal alignment; attributes preserved (type/size/color); reasonable spacing, no overlaps.
- **4 (Near-perfect).** Correct grouping and ordering with one minor imperfection (e.g., small color deviation (hue shift within $\pm 10\%$), small size deviation (within $\pm 5\%$), slight vertical misalignment, or mildly uneven spacing) while the intended layout remains clear.
- **3 (Partially correct).** Grouping is correct but ordering is wrong in at least one group; *or* grouping and ordering are correct but attribute changes are noticeable (e.g., color shift $> 10\%$, size change $> 5\%$, or mild deformation while still recognizable).
- **2 (Multiple errors).** Incorrect grouping and/or incorrect ordering, and/or missing/extra objects.
- **1 (Failure).** Objective not achieved (no intended grouping/ordering) and/or severe object modification/loss.

Evaluation dimensions (suggested weights):

- **Classification accuracy (30%).** Correctly identify the two shape types; group identical shapes; include all 6 objects.
- **Ordering correctness (30%).** Ascending size order within each group; coherent left-to-right organization.
- **Object fidelity (30%).** Preserve shape type, size, and color; maintain clear contours/edges.
- **Layout accuracy (10%).** Horizontal alignment and reasonable spacing.

Grid Avoid Obstacles (Task G-15) Navigate a 10×10 grid from start to goal using only 4-neighbor moves without entering obstacle cells, testing shortest-path planning under hard constraints.

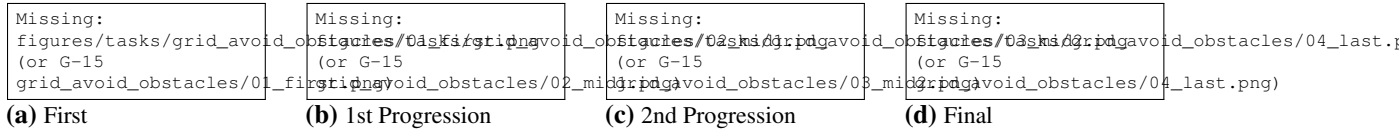


Figure 11 Grid Avoid Obstacles

Example Prompt: “The scene shows a 10x10 grid with a blue start square (containing a yellow circular agent), a red end square, and multiple black X marks indicating obstacles. Starting from the blue start square, the agent can move to adjacent cells (up, down, left, right) each step. The goal is to move the agent to the red end square along the shortest path without entering any cells marked with black X obstacles.”

Human Annotation Scoring (1–5):

- **5 (Perfect).** Reaches the goal; avoids all obstacles; uses a shortest (or tied-shortest) obstacle-avoiding path; movement is legal (4-neighbor, within-grid) and agent appearance is preserved.
- **4 (Near-perfect).** Reaches the goal and avoids all obstacles; only a minor imperfection (e.g., ≤ 2 extra steps vs. optimal, slight appearance drift, or minor legal-motion jitter).
- **3 (Partially correct).** Clear attempt but with a notable issue (e.g., enters exactly one obstacle cell once, > 2 extra steps, stops short of the goal, or an occasional illegal/diagonal tendency).
- **2 (Mostly incorrect).** Multiple violations (e.g., enters 2–3 obstacle cells) and/or out-of-grid motion and/or highly inefficient/random routing and/or fails to reach the goal.
- **1 (Failure).** No meaningful progress or unrelated output; frequent obstacle crossings (≥ 4) or the grid is corrupted.

Evaluation dimensions (suggested weights):

- **Obstacle avoidance (40%).** Zero obstacle entries; respects non-traversable constraint.
- **Path optimality (30%).** Shortest path length under obstacle constraints.
- **Motion-rule compliance (20%).** 4-neighbor steps, within-grid, continuous trajectory.
- **Task completion (10%).** Reaches the goal with a coherent start→goal trajectory.

Directed Graph Navigation (Task G-31) Navigate from the start node to the goal node by traversing only along directed edges (respecting arrow direction) with a minimum-hop path, testing goal-directed graph planning under directionality constraints.

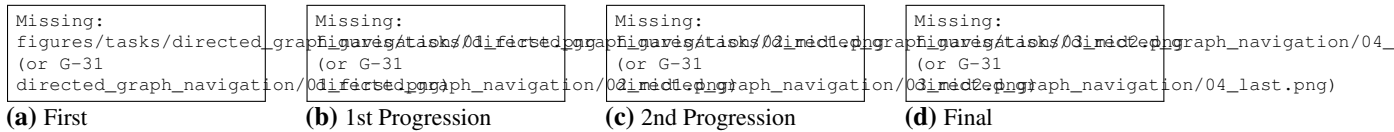


Figure 13 Directed Graph Navigation

Prompt :“The scene shows a network of nodes connected by directed edges (edges with arrows indicating direction) with a green starting node, a red ending node, and a blue triangular agent positioned at the green starting node. The agent can only move along edges in the direction they point (from the source node to the target node, cannot move backwards), moving from one node to an adjacent node each step. Move the blue triangular agent from the green starting node to the red ending node along the path with the minimum number of steps.”

Human Annotation Scoring (1–5):

- **5 (Perfect).** Reaches the goal; uses a minimum-hop path; strictly follows arrow directions and moves only along existing edges; motion is continuous and the graph is preserved.
- **4 (Near-perfect).** Reaches the goal with correct direction/edge-following behavior; only minor presentation issues while path length remains shortest.
- **3 (Partially correct).** Reaches the goal but with a notable issue (e.g., +1–2 extra hops, a single direction violation, or slight deviation from drawn edges).
- **2 (Mostly incorrect).** Severe issues: ≥ 3 extra hops, multiple direction violations, “flying”/cutting across space, reaches the wrong node, or alters graph structure.
- **1 (Failure).** Does not reach the goal, behavior is random/invalid (ignores arrows), or the graph is corrupted.

Evaluation dimensions (suggested weights):

- **Shortest-path correctness (40%).** Minimum-hop path length.
- **Direction compliance (35%).** No reverse traversals; respects arrow orientation.
- **Motion legality (15%).** Moves along existing edges, one edge per step; no teleportation.
- **Graph fidelity (10%).** Nodes/edges/arrows remain unchanged.

Key Door Matching (Task G-45) In a maze, first collect the prompt-specified colored key and then reach the matching door via legal corridor moves near shortest, testing instruction grounding, sequencing, and constrained navigation.

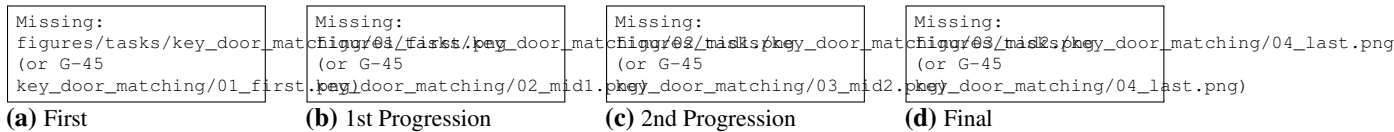


Figure 14 Key Door Matching

Prompt :“The scene shows a maze with a green circular agent, colored diamond-shaped keys, and colored hollow rectangular doors. Find the Blue key and then navigate to the matching Blue door, showing the complete movement process step by step.”

Human Annotation Scoring (1–5):

- **5 (Perfect).** Reaches the correct target-colored key, then reaches the matching door (correct order); path is legal and continuous; path length is near-optimal (e.g., $\leq 120\%$ of BFS shortest for start→key→door); key disappears when reached; full trajectory is shown.
- **4 (Near-perfect).** Correct key and door in correct order; minor issues only (e.g., slightly longer path $\sim 120\%$ – 150% , small jitter/backtracking, or a 1–2 frame delay in key disappearance).
- **3 (Partially correct).** Finds the correct key but makes a major mistake (e.g., goes to wrong door, completes only one stage, noticeably inefficient path $\sim 150\%$ – 200% , or 1–2 minor wall violations).
- **2 (Mostly incorrect).** Wrong key color and/or wrong order (door before key), and/or multiple wall crossings, and/or extremely inefficient path ($> 200\%$), or stops at irrelevant locations.
- **1 (Failure).** Agent barely moves or moves randomly; ignores maze constraints; incorrect key/door colors; or agent behavior is abnormal.

Evaluation dimensions (suggested weights):

- **Target identification (30%).** Correctly identify the prompt-specified key and matching door; do not confuse with other colors.
- **Path validity (30%).** Follow allowed corridors only, avoid wall collisions, and maintain step-by-step movement.
- **Path efficiency (20%).** Actual path length relative to the BFS-optimal path; $\leq 110\%$ = excellent, 110% – 130% = acceptable, $> 200\%$ = poor.
- **Animation quality (20%).** Smooth frame-by-frame movement; agent centers align with key and door; key pickup effect visible.